J. Fluid Mech. (2007), *vol.* 583, *pp.* 347–377.
doi:10.1017/S0022112007006222 Printed in the United Kingdom

Linear stability of a two-fluid interface for electrohydrodynamic mixing in a channel

F. LI[1], O. OZEN[1,2], N. AUBRY[3], D. T. PAPAGEORGIOU[2] AND P. G. PETROPOULOS[2]

[1]Department of Mechanical Engineering, New Jersey Institute of Technology, University Heights, Newark, NJ 07102, USA

[2]Department of Mathematical Sciences and Center for Applied Mathematics and Statistics, New Jersey Institute of Technology, University Heights, Newark, NJ 07102, USA

[3]Department of Mechanical Engineering, Carnegie Mellon University, Pittsburg, PA 15213, USA

(Received 4 April 2006 and in revised form 19 February 2007)

We study the electrohydrodynamic stability of the interface between two superposed viscous fluids in a channel subjected to a normal electric field. The two fluids can have different densities, viscosities, permittivities and conductivities. The interface allows surface charges, and there exists an electrical tangential shear stress at the interface owing to the finite conductivities of the two fluids. The long-wave linear stability analysis is performed within the generic Orr–Sommerfeld framework for both perfect and leaky dielectrics. In the framework of the long-wave linear stability analysis, the wave speed is expressed in terms of the ratio of viscosities, densities, permittivities and conductivities of the two fluids. For perfect dielectrics, the electric field always has a destabilizing effect, whereas for leaky dielectrics, the electric field can have either a destabilizing or a stabilizing effect depending on the ratios of permittivities and conductivities of the two fluids. In addition, the linear stability analysis for all wavenumbers is carried out numerically using the Chebyshev spectral method, and the various types of neutral stability curves (NSC) obtained are discussed.

1. Introduction

Work on the electrohydrodynamic stability of channel flow has recently attracted much attention, particularly because of its use in the field of microfluidics. For instance, in many micro-electro-mechanical-systems (MEMS) devices, rapid mixing is highly desired and can be achieved by applying an electric field, as in the experiments of Moctar, Aubrey & Batton (2003), Glasgow, Batton & Aubry (2004) and Lin *et al.* (2004). Another application is the generation of drops in microchannels in the case of immiscible fluids (Ozen *et al.* 2006*b*). Electrohydrodynamics (EHD) studies the interplay between an electric field and fluid mechanics. One aspect of EHD encompasses, for instance, the influence of the conductivity of the fluids on the stability of a two-fluid layer flow. According to theory, there exist two approaches to this problem: the first is the *bulk coupled* model, which assumes a conductivity gradient in a thin diffusion layer between the two fluids resulting in an electrical body force on the fluids. In a series of studies, Melcher and his coworkers used the bulk coupled model in studying the stability of two fluids stressed by a tangential electric field with conductivity gradient in a diffusive layer (Hoburg & Melcher 1976).

Applications of this approach in microchannels can be found in Lin *et al.* (2004) who analysed the electrokinetic flow in microchannels with conductivity gradients. They performed both linear stability analysis and nonlinear simulations following the framework of Hoburg & Melcher (1976), while also considering the diffusion of conductivity as in Baygents & Baldessari (1998). Storey *et al.* (2005) studied the nonlinear stability using asymptotics, and Chen *et al.* (2005) investigated the absolute and convective instabilities for the same problem. Tardu (2004) carried out the linear stability analysis of a Poiseuille flow under the effect of an electrostatic double layer (EDL) in a microchannel. The second approach is the *surface coupled* model which assumes a jump of conductivity at the interface between the two fluids. This model assumes constant conductivity in each of the fluid layers, and therefore no electric body force in each fluid. Melcher and his coworkers also used the surface coupled model to study the stability of two fluids in an unbounded domain stressed by a tangential electric field (Melcher & Schwarz 1968) and a normal electric field (Melcher & Smith 1969). However, zero mean flow is assumed in their study. When the mean flow is non-zero, even without electric field, the linear stability analysis is difficult since the linearized Navier–Stokes equations reduce to the Orr–Sommerfeld equation for which there is no exact solution. Thus, various asymptotic techniques have been developed to study the interfacial stability of a two-fluid flow.

Yih (1967) first studied two superposed viscous fluids with different viscosities in a channel. He carried out the long-wave linear stability analysis for both Couette flow and Poiseuille flow, and showed that there exists an unstable mode due to viscosity stratification at any Reynolds number, except in some limiting cases, for example, the 'thin-layer effect' discussed by Chen (1995) – see below. This mode, termed the *interfacial mode*, is caused by the jump of fluid viscosity at the interface, and clearly distinguishes itself from the *shear mode* which originates in the mean flow velocity. Asymptotic techniques can be applied to various two-fluid problems, see, for example, the short-wave analysis for Couette flow in an unbounded domain of Hooper & Boyd (1983), the long-wave analysis for Poiseuille flow in a channel of Yiantsios & Higgins (1988) and Hooper (1989), and the study at all wavenumbers and Reynolds numbers in the case where the two fluids have similar mechanical properties (density, viscosity) of Renardy (1987). In general, for Couette flow, the Orr–Sommerfeld equation can be simplified and, in this case, it is possible to obtain solutions by using Airy functions and Airy integrals. In contrast, for Poiseuille flow, asymptotic solutions have to be constructed. A comprehensive summary on the stability analysis of two-fluid systems can be found in Joseph & Renardy (1993). For a more recent review of stratified viscous shear flows (including viscoelastic flows), see Chen (1995) and note his discussion of a lower-viscosity thin-layer stability to long waves effect – this is addressed in the context of electrohydrodynamics in § 4.2 (in particular, in the discussion of figures 14 and 15).

The study of the electrohydrodynamic (EHD) stability of the interface between two superposed fluids in either a confined channel or an unbounded domain under the influence of an electric field has been an active research area since the pioneering work of Melcher & Schwarz (1968) and Melcher & Smith (1969). In this work, we study the EHD stability of two superposed fluids in a channel using the surface coupled model. In this approach, the electric body force vanishes and the electric problem is decoupled from the fluid problem. The electric field changes the tangential and normal shear stress at the interface and thus alters the stability of the flow. Most of the works published in the literature so far have focused on using different asymptotic techniques to derive the dispersion relation. However, numerical results at all wavenumbers

have not been reported. Abdella & Rasmussen (1997) studied Couette flow in the unbounded domain subjected to a normal electric field. They considered two viscous fluids with different viscosities, densities, conductivities and permittivities and used Airy functions and Airy integrals to derive a generic dispersion relation; they studied two special cases in detail: the electrohydrodynamic free-charge configuration (EH-If) (Melcher 1963) and the electrohydrodynamic polarization charge configuration (EH-Ip) (Melcher 1963). Mohamed, Elshehawey & ElSayed (1995) concentrated on two superposed viscous fluids in a channel subjected to a normal electric field where the upper fluid is highly conducting while the lower fluid is dielectric, which is known as the limiting EH-If case where the interface, which is perfectly conducting, carries free charges. The EH-If case is an example where there is no electrical tangential shear stress induced by the electric field at the interface. Mohamed *et al.* (1995) performed the long-wave linear stability analysis following Yih's analysis. The conductivity of the upper fluid is accounted for in their analysis, as well as the polarization forces acting normal to the interface. They discussed both Couette flow and Poiseuille flow subjected to a normal electric field and showed that the electric field always has a destabilizing effect on the flow. As shown later, their work can be treated as a special case of the present study. Tilley, Petropoulos & Papageorgiou (2001) and Savettaseranee *et al.* (2003) studied the rupture of a thin film under the action of an electric field. A review of electrohydrodynamic stability can be found in Saville (1997). Related work on electrohydrodynamic instabilities in liquid sheets, and the ensuing nonlinear features have been investigated by Papageorgiou & Vanden-Broeck (2004) using direct numerical simulations and asymptotics.

In this paper, we perform the linear stability analysis of a two-fluid flow in a channel subjected to a normal electric field. The configuration of our system is generic in that the two fluids are assumed to have different densities, viscosities, permittivities and conductivities. The interface is not perfectly conducting and admits free charges because the two fluids have finite conductivities. We first derive the long-wave asymptotic dispersion relation and then present numerical calculations using the Chebyshev spectral method valid for all wavenumbers. This paper is organized as follows. In § 2, we present the mathematical formulation of our EHD problem; in § 3, we perform the long-wave linear stability analysis, derive the wave-speed eigenvalue and then discuss the influence of the electric field on the two-fluid system in detail; in § 4, we present results of our numerical calculations for the linearized electrohydrodynamic problem valid for all wavenumbers, and finally draw our conclusions in § 5.

2. The physical and mathematical model

We consider a two-layer system of two superimposed conducting viscous fluids in a long channel (figure 1). The lower fluid is referred to as fluid 1, while the upper fluid is denoted fluid 2. Fluid j ($j = 1, 2$) is assumed to have density ρ_j, dynamic viscosity μ_j, electric permittivity ε_j and electric conductivity σ_j. Here in after, x denotes the streamwise direction, while y refers to the direction normal to the walls. The origin of the y-axis is chosen to coincide with the initial interface between the two fluids so the initial interface is at $y = 0$. The initial height of the lower fluid layer is h_1 and that of the upper fluid layer is h_2. When considering Couette flow, the upper wall of the channel is assumed to have a constant horizontal velocity U_0, while the lower wall is fixed. Accordingly, the mean horizontal velocities of the fluids are denoted by $U^{(1)}(y)$ and $U^{(2)}(y)$. The two fluids are assumed to be incompressible, and the flow

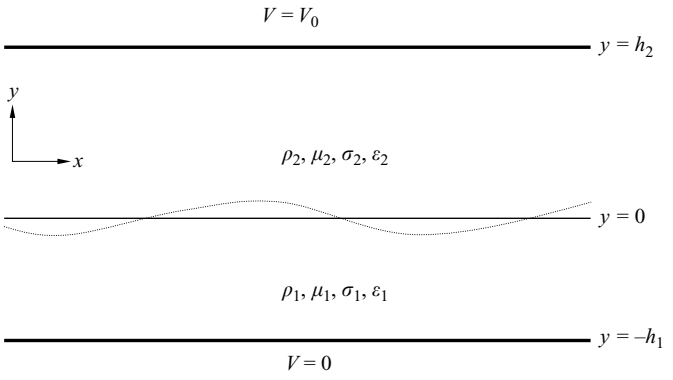

FIGURE 1. Schematic of the physical problem.

is two-dimensional. The equations of motion are given by the continuity and the Navier–Stokes equations

$$\nabla \cdot \boldsymbol{u}^{(j)} = 0, \tag{2.1}$$

$$\rho_j \left[\frac{\partial \boldsymbol{u}^{(j)}}{\partial t} + \left(\boldsymbol{u}^{(j)} \cdot \nabla\right) \boldsymbol{u}^{(j)} \right] = -\nabla p_j - \rho_j g \boldsymbol{y} + \mu_j \nabla^2 \boldsymbol{u}^{(j)}, \tag{2.2}$$

where $j = 1, 2$, refers to fluids 1 and 2, respectively, and $\boldsymbol{u}^{(j)} = u^{(j)}\boldsymbol{x} + v^{(j)}\boldsymbol{y}$ is the velocity field. Throughout this work, we use the surface coupled model rather than the bulk coupled model. The permittivity and conductivity are assumed to be constant in each fluid, and thus the body force induced by the electric field vanishes in the bulk of each fluid. The coupling between the motion of the two fluids occurs through a jump of permittivity and conductivity across the interface.

The fluid velocity satisfies the no-slip boundary condition at both the upper and lower walls, i.e.

$$u^{(2)}(h_2) = U_0,\ v^{(2)}(h_2) = 0, \tag{2.3}$$

$$u^{(1)}(-h_1) = 0,\ v^{(1)}(-h_1) = 0. \tag{2.4}$$

The interface between the two fluids is defined by $F(x, y, t) = y - S(x, t) = 0$ and the unit vector $\boldsymbol{n}_s$, outward normal to the interface, can be written as $\boldsymbol{n}_s = \nabla F/|\nabla F| = (-S_x\boldsymbol{x} + \boldsymbol{y})(1 + S_x^2)^{-1/2}$. At the interface between the two fluids, the velocity meets the kinematic constraint that the fluids move with the interface $y = S(x, t)$, so that

$$S_t + S_x u^{(j)} = v^{(j)}, \qquad y = S(x, t). \tag{2.5}$$

The two walls are both solid boundaries and electrodes. The upper wall is energized at the constant electric potential V_0 while the lower one is grounded so that its electric potential is zero. The two fluids are thus subjected to a normal electric field $\boldsymbol{E}^{(j)} = -\nabla V^{(j)}$, $(j = 1, 2)$. The electric potentials $V^{(j)}(x, y, t)$ satisfy the Laplace equation

$$\nabla^2 V^{(j)} = 0, \tag{2.6}$$

with the following boundary conditions on the upper and lower walls

$$V^{(2)}(h_2) = V_0, \tag{2.7}$$

$$V^{(1)}(-h_1) = 0. \tag{2.8}$$

The continuity of the tangential component of the electric field at the interface reads

$$\boldsymbol{n}_s \times \left[\nabla V^{(j)}\right]_2^1 = 0, \tag{2.9}$$

where the bracket is defined by $[A^{(j)}]_2^1 = A^{(1)} - A^{(2)}$, $A^{(j)}(j = 1, 2)$ being any scalar or vector variable. The above condition can be written as

$$S_x \left[V_y^{(j)}\right]_2^1 + \left[V_x^{(j)}\right]_2^1 = 0, \qquad y = S(x, t).$$

For leaky dielectrics, the conservation equation for the interfacial charge reduces to

$$\boldsymbol{n}_s \cdot \left[\sigma_j \nabla V^{(j)}\right]_2^1 = 0 \quad (j = 1, 2). \tag{2.10}$$

when the ratio of the fluid to electric time scales

$$\frac{\tau^F}{\tau^E} = \frac{\mu h/\gamma}{\varepsilon_0/\sigma} \tag{2.11}$$

is large. Equation (2.10) can be further rewritten as

$$S_x \left[\sigma_j V_x^{(j)}\right]_2^1 = \left[\sigma_j V_y^{(j)}\right]_2^1, \qquad y = S(x, t).$$

Notice that for perfect dielectrics with no surface charges at the interface, the boundary condition (2.10) is replaced by the continuity of the normal component of the displacement field $\varepsilon_j \boldsymbol{E}^{(j)}$ $(j = 1, 2)$. This is effectively obtained by replacing the conductivities σ_j with the permittivities ε_i of the two fluids.

There are four important boundary conditions at the interface $y = S(x, t)$ given by the continuity of the tangential and normal velocity components, and the continuity of the tangential and normal stresses. The continuity of the tangential and normal velocity components across the interface leads to

$$u^{(1)} = u^{(2)}, \qquad y = S(x, t), \tag{2.12}$$

$$v^{(1)} = v^{(2)}, \qquad y = S(x, t). \tag{2.13}$$

The surface stress is composed of the hydrostatic pressure, the viscous stress and the electrical stress. The stress tensor $\tau_{lm}^{(j)}$ is expressed by

$$\tau_{lm}^{(j)} = -p_j \delta_{lm} + \mu_j \left(\frac{\partial u_l^{(j)}}{\partial x_m} + \frac{\partial u_m^{(j)}}{\partial x_l} \right) + M_{lm}^{(j)},$$

where $j = 1, 2$ refers to fluids 1 and 2. Here, p_j $(j = 1, 2)$ denotes the hydrostatic pressure, δ_{lm} is the Kronecker delta symbol, and $M_{lm}^{(j)}$ represents the electric Maxwell stress tensor whose expression is

$$M_{lm}^{(j)} = \varepsilon_j E_l^{(j)} E_m^{(j)} - \tfrac{1}{2} \varepsilon_j E_l^{(j)} E_l^{(j)} \delta_{lm},$$

which shows that $M_{11}^{(j)} = \frac{1}{2}\varepsilon_j [(E_1^{(j)})^2 - (E_1^{(j)})^2]$, $M_{12}^{(j)} = M_{21}^{(j)} = \varepsilon_j E_1^{(j)} E_2^{(j)}$, $M_{22}^{(j)} = \frac{1}{2}\varepsilon_j [(E_2^{(j)})^2 - (E_1^{(j)})^2]$, where $E_1^{(j)} = \partial V^{(j)}/\partial x$, $E_2^{(j)} = \partial V^{(j)}/\partial y$.

The tangential shear stress consists of the balance between the viscous stress and the electrical stress such that

$$\left[S_x \left(\tau_{22}^{(j)} - \tau_{11}^{(j)}\right) + \left(1 - S_x^2\right) \tau_{12}^{(j)}\right]_2^1 = 0, \tag{2.14}$$

while the normal stress at the interface, balanced by the surface tension, takes the expression

$$\left[S_x^2 \tau_{11}^{(j)} - 2 S_x \tau_{12}^{(j)} + \tau_{22}^{(j)}\right]_2^1 = T S_{xx} \left(1 + S_x^2\right)^{-1/2}, \tag{2.15}$$

where T is the surface tension coefficient.

Equations (2.1)–(2.15) comprise our mathematical model for the electrohydrodynamic problem. We now non-dimensionalize the system of equations with the length scale L, the velocity at the interface U_{int} and the constant electric potential V_0. The dimensionless variables are:

$$x^* = \frac{x}{L}, \quad y^* = \frac{y}{L}, \quad S^* = \frac{S}{L}, \quad t^* = \frac{tU_{int}}{L}, \quad U^{(j)*}(y) = \frac{U^{(j)}(y)}{U_{int}}, \quad \eta_1 = \frac{h_1}{L}, \quad \eta_2 = \frac{h_2}{L},$$

$$\mu = \frac{\mu_2}{\mu_1}, \quad \rho = \frac{\rho_2}{\rho_1}, \quad \varepsilon = \frac{\varepsilon_2}{\varepsilon_1}, \quad \sigma = \frac{\sigma_2}{\sigma_1}, \quad n = \frac{h_2}{h_1}, \quad V^{(j)*}(x, y, t) = \frac{V^{(j)}(x, y, t)}{V_0},$$

$$p^* = \frac{p}{\rho_1 U_{int}^2}, \quad F = \frac{U_{int}^2}{gL}, \quad T = \frac{T_0}{\rho_1 U_{int}^2 L}, \quad E_b = \frac{\varepsilon_1 V_0^2}{\rho_1 U_{int}^2 L^2}, \quad Re_j = \frac{\rho_j U_{int} L}{\mu_j},$$

where $j = 1, 2$ refers to fluids 1 and 2, and the superscript $*$, which denotes the dimensionless variables, will later be dropped from the equations. For flow in a bounded domain such as a channel, the typical length L can be any dimensional length of the system. For instance, Yih (1967) used the height of the upper fluid layer h_2, i.e. $L = h_2$, Hooper (1989) used the height of the lower fluid layer h_1, i.e. $L = h_1$, whereas Renardy (1985) used the height of the whole channel, i.e. $L = h_1 + h_2$. When the two fluid layers are of the same height in the channel, we have $\eta_1 = \eta_2 = 1$ with L being either h_1 or h_2. For a flow in an unbounded domain, the typical length L can be any well-defined dimensional length. In our calculations, the length scale is chosen to be the height of the lower fluid, h_1. Furthermore, the ratio of the initial heights of the two fluids is n, the viscosity ratio μ, the density ratio ρ, the permittivity ratio ε, and the conductivity ratio σ. The dimensionless parameters consist of the Reynolds numbers in each fluid layer Re_1 and Re_2 with $Re_2/Re_1 = \rho/\mu$, the Froude number F accounting for the gravity effect, the surface tension parameter T, and the ratio of the electric-field-induced pressure to the inertial forces E_b. Note that when the electric field is turned off, $E_b = 0$.

An exact solution of the Navier–Stokes equations driven by a constant pressure gradient and a constant wall velocity (i.e. a mixed Poiseuille/Couette flow) is given, in dimensionless form, by

$$U^{(1)}(y) = A_1 y^2 + a_1 y + 1, \quad -\eta_1 \leqslant y \leqslant 0, \tag{2.16}$$

$$U^{(2)}(y) = A_2 y^2 + a_2 y + 1, \quad 0 \leqslant y \leqslant \eta_2, \tag{2.17}$$

where the coefficients, determined from the wall and interfacial boundary conditions, are $A_2 = (\mu\eta_1 u_n - (\mu\eta_1 + \eta_2))/\mu\eta_1\eta_2(\eta_1 + \eta_2)$, $A_1 = \mu A_2$, $a_2 = (\mu\eta_1^2 u_n + \eta_2^2 - \mu\eta_1^2)/\mu\eta_1\eta_2(\eta_1 + \eta_2)$ and $a_1 = \mu a_2$. For Couette flow, the velocity profile is linear and the upper wall moves with velocity $u_n = (\mu\eta_1 + \eta_2)/\mu\eta_1$; for Poiseuille flow, the upper wall is fixed and $u_n = 0$.

The resulting dimensionless system of equations is summarized in Appendix A.

3. Linear stability analysis

In this section, we perform the long-wave linear stability analysis of the above EHD problem. For this purpose, we use the normal mode method and assume that the interface S takes the form $S = \hat{s}\exp(\mathrm{i}k(x - ct))$, where $\hat{s}$ is the complex surface amplitude, k is a real number denoting the wavenumber, $c = c_r + \mathrm{i}c_i$ is a complex number representing the wave speed, and $c_i k$ refers to the growth rate which determines the stability property of the system. Specifically, when $c_i < 0$, the system is stable, when $c_i > 0$, the system is unstable and when $c_i = 0$, the system is neutrally

stable. We next present the linear equations and deduce asymptotically the solution of the eigenvalue problem valid for long waves ($k \to 0$).

We first notice that the equations of the electric field (see Appendix A, (A9)–(A13)) are decoupled from those of the flow field and can thus be solved independently. The basic state electric potential $V_0^{(j)}(y)$ is obtained by solving the Laplace equations in the two fluid layers to yield

$$V^{(1)}(x, y, t) = \frac{\sigma y + \sigma\eta_1}{\eta_2 + \sigma\eta_1} + \chi^{(1)}(x, y, t),$$
$$V^{(2)}(x, y, t) = \frac{y + \sigma\eta_1}{\eta_2 + \sigma\eta_1} + \chi^{(2)}(x, y, t),$$

where the first terms are the basic states and $\chi^{(j)}$ ($j = 1, 2$) are the perturbed electric potentials, which also satisfy the Laplace equation $\nabla^2\chi^{(j)} = 0$. The linearized system for the perturbed electric potential $\chi^{(j)}$ reads

$$\chi_{xx}^{(j)} + \chi_{yy}^{(j)} = 0, \quad j = 1, 2, \tag{3.1}$$
$$\chi^{(1)}(-\eta_1) = 0, \tag{3.2}$$
$$\chi^{(2)}(\eta_2) = 0, \tag{3.3}$$
$$S_x \frac{\sigma - 1}{\eta_2 + \sigma\eta_1} + \left(\chi_x^{(1)} - \chi_x^{(2)}\right) = 0 \quad \text{on} \quad y = 0, \tag{3.4}$$
$$\chi_y^{(1)} = \sigma\chi_y^{(2)} \quad \text{on} \quad y = 0. \tag{3.5}$$

The solutions of $\chi^{(j)}(j = 1, 2)$ are also expressed in the form of normal modes to obtain

$$\chi^{(1)} = -\frac{\hat{s}(\sigma - 1)\sigma}{(\tanh k\eta_2 + \sigma \tanh k\eta_1)(\eta_2 + \sigma\eta_1)} \frac{\sinh k(y + \eta_1)}{\cosh k\eta_1} \exp(\mathrm{i}k(x - ct)), \tag{3.6}$$
$$\chi^{(2)} = -\frac{\hat{s}(\sigma - 1)}{(\tanh k\eta_2 + \sigma \tanh k\eta_1)(\eta_2 + \sigma\eta_1)} \frac{\sinh k(y - \eta_2)}{\cosh k\eta_2} \exp(\mathrm{i}k(x - ct)). \tag{3.7}$$

Regarding the flow field, we linearize the Navier–Stokes equations using $u^{(j)} = U^{(j)} + u'^{(j)}$, $v^{(j)} = v'^{(j)}$, $p^{(j)} = p_0^{(j)} + p'^{(j)}$ ($j = 1, 2$), where the primes denote small perturbation variables and $p_0^{(1)} = -y/F$, $p_0^{(2)} = -\rho y/F$. Using the streamfunction $\psi^{(j)}(x, y, t)$ related to the velocity perturbations by $u'^{(j)} = \partial\psi^{(j)}/\partial y$, $v'^{(j)} = -\partial\psi^{(j)}/\partial x$, and assuming $\psi^{(j)}(x, y, t) = \phi^{(j)}(y)\exp(\mathrm{i}k(x - ct))$, where $\phi^{(j)}(y)$ is the complex amplitude, the Navier–Stokes equations are linearized to give the usual Orr–Sommerfeld equation for fluids 1 and 2. In summary, we have obtained the following linearized system of equations and boundary conditions for the two streamfunction amplitudes $\phi^{(1)}$ and $\phi^{(2)}$:

$$\left(\frac{\mathrm{d}^2}{\mathrm{d}y^2} - k^2\right)^2 \phi^{(1)} = \mathrm{i}kRe_1 \left[\left(U^{(1)} - c\right)\left(\frac{\mathrm{d}^2}{\mathrm{d}y^2} - k^2\right)\phi^{(1)} - \phi^{(1)}\frac{\mathrm{d}^2U^{(1)}}{\mathrm{d}y^2}\right], \tag{3.8}$$
$$\left(\frac{\mathrm{d}^2}{\mathrm{d}y^2} - k^2\right)^2 \phi^{(2)} = \mathrm{i}kRe_2 \left[\left(U^{(2)} - c\right)\left(\frac{\mathrm{d}^2}{\mathrm{d}y^2} - k^2\right)\phi^{(2)} - \phi^{(2)}\frac{\mathrm{d}^2U^{(2)}}{\mathrm{d}y^2}\right], \tag{3.9}$$
$$\phi^{(1)}(-\eta_1) = \phi_y^{(1)}(-\eta_1) = 0, \tag{3.10}$$
$$\phi^{(2)}(\eta_2) = \phi_y^{(2)}(\eta_2) = 0, \tag{3.11}$$
$$\phi^{(1)}(0) = \phi^{(2)}(0) = \phi(0), \tag{3.12}$$

$$\frac{\mathrm{d}\phi^{(1)}}{\mathrm{d}y}(0) - \frac{\mathrm{d}\phi^{(2)}}{\mathrm{d}y}(0) = \frac{\phi(0)}{c-1}(a_2 - a_1), \tag{3.13}$$

$$\left(\frac{\mathrm{d}^2}{\mathrm{d}y^2} + k^2\right)\phi^{(1)} - \mu\left(\frac{\mathrm{d}^2}{\mathrm{d}y^2} + k^2\right)\phi^{(2)} + \mathrm{i}kRe_1E_bQ_T\hat{s} = 0 \quad \text{on} \quad y = 0, \tag{3.14}$$

$$\left(\frac{\mathrm{d}^2}{\mathrm{d}y^2} - 3k^2\right)\frac{\mathrm{d}\phi^{(1)}}{\mathrm{d}y} - \mu\left(\frac{\mathrm{d}^2}{\mathrm{d}y^2} - 3k^2\right)\frac{\mathrm{d}\phi^{(2)}}{\mathrm{d}y}, + \mathrm{i}kRe_1(\rho Q_0 - k^2T\hat{s} - E_bQ_N\hat{s}) = 0 \quad \text{on} \quad y = 0, \tag{3.15}$$

where Q_0, Q_T, Q_N are given by

$$Q_0 = \frac{\rho - 1}{\rho F}\hat{s} + (c-1)\left(\frac{1}{\rho}\frac{\mathrm{d}\phi^{(1)}}{\mathrm{d}y} - \frac{\mathrm{d}\phi^{(2)}}{\mathrm{d}y}\right) + \phi(0)\left(\frac{1}{\rho}a_1 - a_2\right), \tag{3.16}$$

$$Q_T = \frac{1}{(\eta_2 + \sigma\eta_1)^2}\left[(\sigma^2 - \varepsilon) - (\sigma - 1)\frac{\varepsilon\tanh k\eta_2 + \sigma^2\tanh k\eta_1}{\tanh k\eta_2 + \sigma\tanh k\eta_1}\right], \tag{3.17}$$

$$Q_N = \frac{(\sigma - 1)(\varepsilon - \sigma^2)}{(\eta_2 + \sigma\eta_1)^2}\frac{k}{\tanh k\eta_2 + \sigma\tanh k\eta_1}. \tag{3.18}$$

Here, Q_0 represents the effect of gravity, while Q_T and Q_N represent the influence of the electric field on the tangential and normal stress balance at the interface, respectively. For the electrical tangential shear stress factor Q_T, there are two limiting cases, which we now discuss. The first case is that of perfect dielectrics without surface charges at the interface (EH-Ip) (Melcher 1963), for which we replace σ by ε, leading to $Q_T = 0$. In this case, we thus recover the result that perfect dielectrics do not induce electrical tangential shear stresses, but only normal electrical stresses at the interface. The second limiting case corresponds to a perfectly conducting surface in the situation where one fluid has a much higher conductivity than the other. It follows that the charge relaxation time is short compared with the typical mechanical time scale (EH-If)) (Melcher 1963), i.e. $\sigma \to 0$ (or $\sigma \to \infty$), in which case we also have $Q_T \to 0$, thus recovering the result that the electrical tangential shear stress vanishes at the interface (Mohamed *et al.* 1995). However, for leaky dielectrics with surface charges at the interface and two fluids that are not perfectly conducting, we must bear in mind that there is an electrical tangential shear stress at the interface, induced by the electric field. As we will see in the analysis below, the presence of an electrical tangential shear stress greatly changes the stability of the two-fluid-layer system as previously investigated by Ozen *et al.* (2006*a*). Ozen and his coworkers have looked at the effect, of an electric field on the instability of an interface between two immiscible liquids in channel flow, where the interface admits free charge (Ozen *et al.* 2006*a*). Similar findings have also been reported by Papageorgiou & Petropoulos (2004) and Ozen *et al.* (2006*c*), in the related problem of fluid sheets stressed by a horizontal electric field (linear and nonlinear theories are presented) – the field effect is typically stabilizing in such configurations unless the leaky dielectric model is used.

Another observation from the above linearized results is that when $\varepsilon = \sigma^2$, then $Q_N = 0$ but $Q_T \neq 0$, which implies that the electrical normal stress at the interface could vanish while the electrical tangential shear stress is still present. The stability of the flow will then be driven by the electrical tangential shear stress alone when $\varepsilon = \sigma^2$. Furthermore, depending on $\varepsilon > \sigma^2$ or $\varepsilon < \sigma^2$, the normal electrical stress acts in different directions across the interface, an issue which will be discussed in more detail when we present the results of our numerical calculations.

3.1. *Long-wave asymptotics*

We now carry out the long-wave linear stability analysis which is valid for $k \to 0$, and expand $\phi^{(1)}$, $\phi^{(2)}$, c, $\hat{s}$ as follows:

$$\phi^{(1)} = \phi_0^{(1)} + k\phi_1^{(1)} + O(k^2), \quad \phi^{(2)} = \phi_0^{(2)} + k\phi_1^{(2)} + O(k^2),$$
$$c = c_0 + kc_1 + O(k^2), \quad \hat{s} = \hat{s}_0 + k\hat{s}_1 + O(k^2).$$

Using the kinematic constraint condition (2.5) at the interface, we can write $S_t + U^{(1)}S_x = v^{(1)}$, which gives $\hat{s} = \phi^{(1)}(0)/(c - U^{(1)}(0)) = \phi(0)/(c-1)$ and $\hat{s}_0 = 1/(c_0 - 1)$, $\hat{s}_1 = -c_1/(c_0-1)^2$, where we have used the facts that $\phi^{(1)}(0) = \phi^{(2)}(0) = \phi(0) = 1$ and $U^{(1)}(0) = U^{(2)}(0) = 1$. Since the electric field enters through the boundary conditions of the tangential and normal stress balance at order k, it does not affect the leading-order problem. We also observe that the surface tension appears at the higher order $O(k^3)$, which implies that it does not affect the long-wave result, but plays an important role in stabilizing sufficiently short waves. The leading-order problem, first studied by Yih (1967), is given by

$$c_0 - 1 = Q_L(\mu, \eta_1, \eta_2)(a_2 - a_1), \tag{3.19}$$

where

$$Q_L(\mu, \eta_1, \eta_2) = \frac{2\mu\eta_1^2\eta_2^2(\eta_1 + \eta_2)}{\mu^2\eta_1^4 + \eta_2^4 + 2\mu\eta_1\eta_2(2\eta_1^2 + 3\eta_1\eta_2 + 2\eta_2^2)}. \tag{3.20}$$

Note that we have used a different convention from Yih and his result can be recovered by replacing μ by $1/\mu$.

For simplicity of presentation, we have deferred the solution of the first-order problem to Appendix B. This solution gives the following first-order correction to the eigenvalue c:

$$c_1 = \mathrm{i}Re_2(J_0 + J_E), \tag{3.21}$$

where $Re_2 = Re_1\rho/\mu$ is the Reynolds number of the upper fluid and

$$J_0 = \mu Q_L^2(a_2 - a_1)H_{12}, \tag{3.22}$$

$$J_E = -\mu Q_L\left[\frac{\eta_1\eta_2((1/\mu)\eta_2 + \eta_1)}{6(\eta_1 + \eta_2)}Q_N + \frac{(1/\mu)\eta_2^2 - \eta_1^2}{4(\eta_1 + \eta_2)}Q_T\right]\frac{E_b}{\rho}. \tag{3.23}$$

The first term is that first obtained by Yih (1967) in the absence of an electric field. The details of H_{12} in the expression of J_0 can be found in Appendix B. The second term containing J_E represents the correction of the electric field to the first-order eigenvalue c_1. Note that J_E is not related to the velocity profile of the mean flow, but depends on ε, σ, μ, η_1 and η_2, and increases linearly with E_b. The electric field has a destabilizing (stabilizing) effect on the flow field when $J_E > 0$ ($J_E < 0$).

It is worth pointing out that in the absence of an electric field $E_b = 0$, J_E is also equal to zero and the two-fluid system can be neutrally stable when $J_0 = 0$. This occurs when $\mu = 1$, $\mu = n^2$ for Poiseuille flow and when $\mu = 1$ for Couette flow. Since the neutrally stable mode implies that there is no viscous tangential shear stress at the interface, and since for leaky dielectrics without a perfectly conducting interface (σ_1, σ_2 finite) an electrical tangential shear stress is induced across the interface, the mathematical model of the EHD problem does not hold for leaky dielectrics without a perfectly conducting interface in these special cases. This is because the induced electrical tangential shear stress at the interface is no longer balanced by the viscous tangential shear stress. There is thus a need for other models to study the impact of the electric field on the neutrally stable modes for leaky dielectrics without a

perfectly conducting interface. However, our model is still valid for perfect dielectrics (σ replaced by ε) or for perfectly conducting interfaces where $\sigma \to 0$ or $\sigma \to \infty$.

We now investigate the electric field effects on the stability of the flow in the long-wave regime. Using (3.21), we obtain instability when $(J_0 + J_E) > 0$ and stability when $(J_0 + J_E) < 0$. In addition, J_E can be rewritten as

$$J_E = -\mu Q_L \left[\frac{\eta_1\eta_2((1/\mu)\eta_2+\eta_1)}{6(\eta_1+\eta_2)} \frac{(\sigma-1)(\varepsilon-\sigma^2)}{(\eta_2+\sigma\eta_1)^3} + \frac{(1/\mu)\eta_2^2-\eta_1^2}{4} \frac{\sigma(\sigma-\varepsilon)}{(\eta_2+\sigma\eta_1)^3} \right] \frac{E_b}{\rho}, \quad (3.24)$$

with Q_L given by (3.20). For perfect dielectrics (i.e. no charges at the interface), we replace σ by ε as explained earlier, to obtain

$$J_E = \mu Q_L \frac{\eta_1\eta_2((1/\mu)\eta_2+\eta_1)}{6(\eta_1+\eta_2)} \frac{\varepsilon(\varepsilon-1)^2}{(\eta_2+\varepsilon\eta_1)^3} \frac{E_b}{\rho} > 0. \quad (3.25)$$

It follows that for perfect dielectrics, the electric field is always destabilizing for the problem studied here. In this limit, there are no electrical tangential shear stresses at the interface (EH-Ip). Another situation where the electric field does not induce a tangential shear stress, is the case where the interface is perfectly conducting (EH-If) and supports surface charges, as in Mohamed *et al.* (1995). Their result is a special case of ours and is recovered by setting $\sigma \to \infty$ in (3.24) so that

$$J_E = \mu Q_L \frac{\eta_2((1/\mu)\eta_2+\eta_1)}{6\eta_1^2(\eta_1+\eta_2)} \frac{E_b}{\rho} > 0. \quad (3.26)$$

Hence, the electric field is again destabilizing. A similar conclusion can be drawn in the limiting case $\sigma \to 0$.

In contrast to these findings, for leaky dielectrics where the finite conductivity of the fluid plays a role and a tangential shear stress is present at the interface, the electric field can have either a destabilizing or a stabilizing effect, depending on the ratio of conductivities and permittivities of the two fluids. In order to further analyse the expression (3.24) of J_E, we set $\eta_2 = n$, $\eta_1 = 1$, define

$$\alpha = \frac{\eta_1\eta_2((1/\mu)\eta_2+\eta_1)}{6(\eta_1+\eta_2)} = \frac{n(n/\mu+1)}{6(n+1)}, \quad \beta = \frac{(1/\mu)\eta_2^2-\eta_1^2}{4} = \frac{n^2/\mu-1}{4}, \quad (3.27)$$

and rewrite J_E as

$$J_E = -\frac{\mu Q_L}{(n+\sigma)^3}[\alpha(\sigma-1)(\varepsilon-\sigma^2)+\beta\sigma(\sigma-\varepsilon)]\frac{E_b}{\rho}. \quad (3.28)$$

It is then clear that the sign of J_E depends on the specific values of σ, ε, μ and n. Since $\alpha > 0$ holds for all μ and n, we consider the effect of β on the sign of J_E. The following representative cases are of interest:

(I) $\beta < 0$, i.e. $\mu > n^2$. In this case, the curve $J_E = 0$ is shown in figure 2 in the σ, ε domain for representative parameters (*a*) $\mu = 2$, $n = 0.8$ and (*b*) $\mu = 0.25$, $n = 0.2$. Note that the curve $J_E = 0$ has a vertical asymptote $\sigma = \alpha/(\alpha - \beta)$ indicated on the figures by a dashed line.

(II) $\beta > 0$, i.e. $\mu < n^2$. In this case, the sign of J_E depends not only on ε and σ, but also on the relative value of α and β (i.e. μ and n).

(*i*) Figure 3 gives representative results for the case where $\alpha > \beta$ and (*a*) $\mu = 8.0$, $n = 3.0$, (*b*) $\mu = 0.1$, $n = 1/3$. The curve $J_E = 0$ has a vertical asymptote as before.

(*ii*) Figure 4 shows two other examples with $\alpha < \beta$ for the parameters (*a*) $\mu = 0.5$, $n = 2.0$ and (*b*) $\mu = 0.1$, $n = 0.5$. The curve $J_E = 0$ has no vertical asymptote in this case.

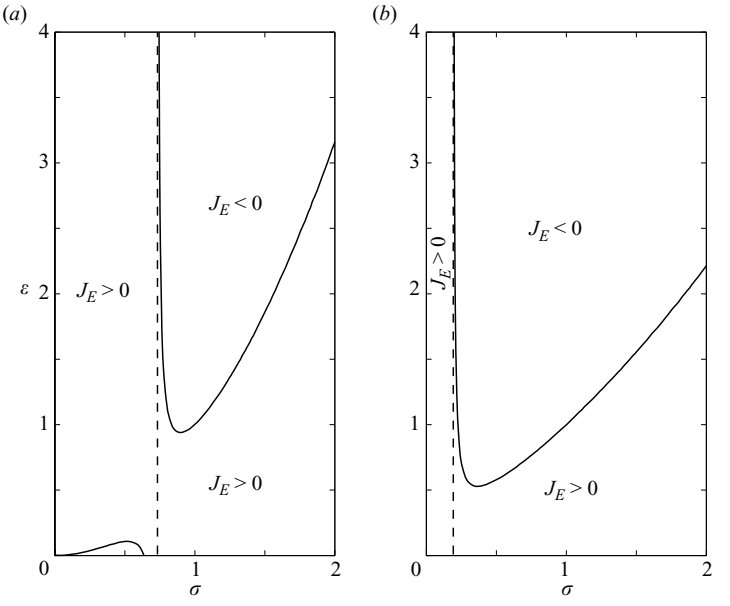

FIGURE 2. Long-wave analysis. The curve $J_E = 0$ is represented in the (ε, σ)-plane for two cases where $\mu > n^2$: (*a*) $\mu = 2$, $n = 0.8$; (*b*) $\mu = 0.25$, $n = 0.2$.

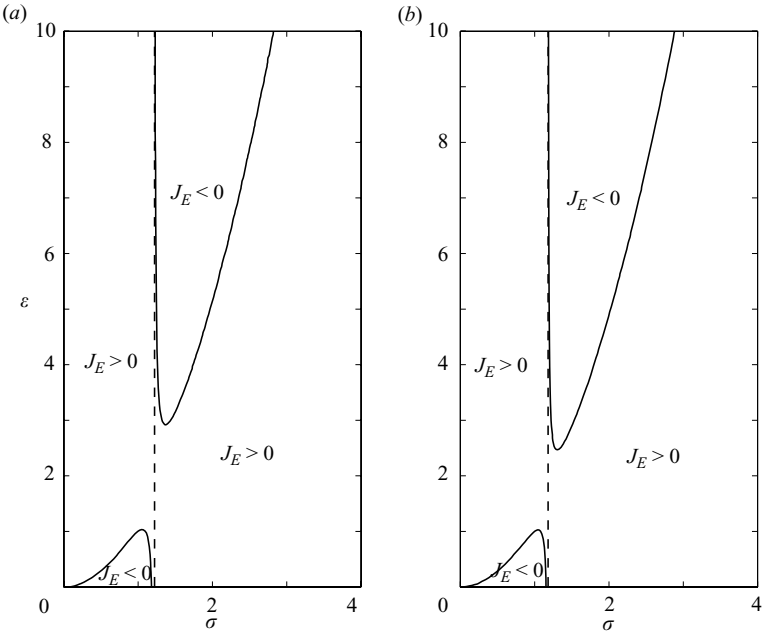

FIGURE 3. Long-wave analysis. The curve $J_E = 0$ is represented in the (ε, σ)-plane for two cases where $\mu < n^2$ and $\alpha > \beta$: (*a*) $\mu = 8$, $n = 3$; (*b*) $\mu = 0.1$, $n = 1/3$.

(III) $\beta = 0$, i.e. $\mu = n^2$. As we discussed earlier, our model cannot be applied to a Poiseuille flow having a neutral stable mode. The model is valid for Couette flow, however, and the sign of J_E is determined by $(\sigma - 1)(\varepsilon - \sigma^2)$ alone. The sign of J_E for

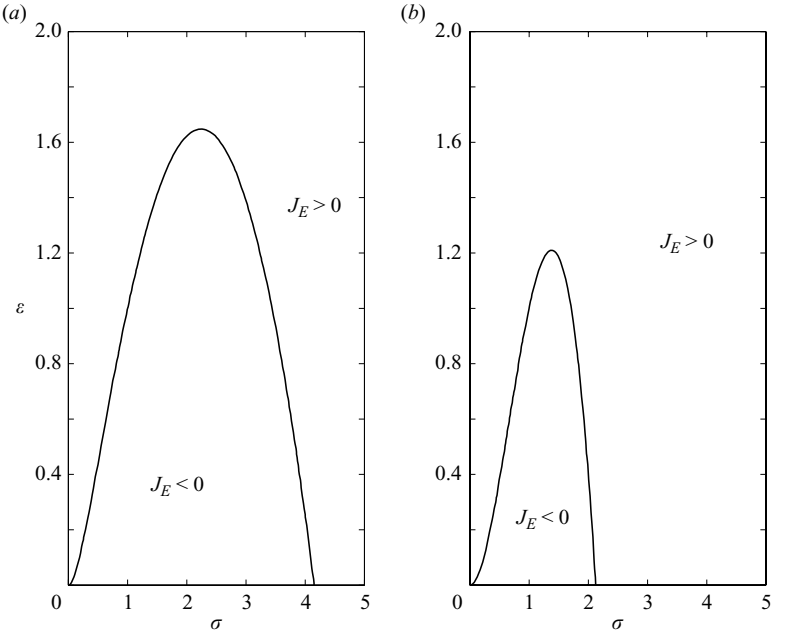

FIGURE 4. Long-wave analysis, curve $J_E = 0$ in the (ε, σ)-plane when $\mu < n^2$ and $\alpha < \beta$. (*a*) $\mu = 0.5$, $n = 2$; (*b*) $\mu = 0.1$, $n = 0.5$.

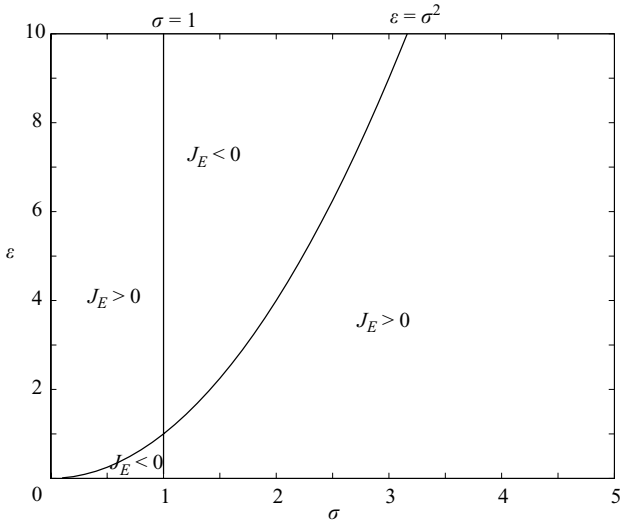

FIGURE 5. Long-wave analysis. The curve $J_E = 0$ is represented in the (ε, σ)-plane with $\mu = n^2$. This is for the case of Couette flow only.

$\mu = n^2$ can be identified in figure 5 where the curve $J_E = 0$ is displayed in the (σ, ε) plane. It is clear that with different choices for σ and ε, J_E can be either positive or negative, so the flow can be either stabilized or destabilized by the electric field.

Note that the electric field can have a stabilizing effect on the system. As our analysis shows, this stabilizing effect is a result of the tangential shear stress induced

by the electric field. It has been pointed out by Melcher & Smith (1969) that it is inconsistent to ignore electrical shear forces in finite conductivity viscous flows. Indeed, when the interface supports free charges but is not perfectly conducting, electrical shear forces are important and cannot be neglected. Furthermore, an inviscid model is not expected to produce accurate results in these types of problems.

Next, we discuss the behaviour of J_E in the limit where the viscosity of one of the fluids approaches zero or infinity. If the electric field is absent, the system has a neutrally stable interfacial mode. When the viscosity of one of the fluids becomes very small, supposing that the viscosity of the top fluid goes to zero and thus $\mu = \mu_2/\mu_1 \to 0$, we find that J_E is of order μ ($Q_L = O(\mu)$ also). However, when $\mu_2 \to 0$, $Re_2 \sim O(1/\mu)$, we deduce from (3.21) that the electric field contribution to the first-order correction c_1 is of order 1, i.e. $Re_2 J_E = O(1)$. This implies that when the top fluid is much less viscous, the electric field can still have a significant effect on the flow stability. Similar conclusions can be drawn for the case $\mu \to \infty$ where the viscosity of the top fluid becomes very large.

The stability characteristics described in this section are indicative of the flow development at small wavenumbers. Computational studies must be undertaken, however, in order to calculate the stability characteristics at arbitrary values of k, and this is performed in the remainder of the paper.

4. Spectral method for the linear problem

In this section, we solve the linear electrohydrodynamics problem numerically for all wavenumbers. For this purpose, we use the Chebyshev tau QZ algorithm to discretize the system of equations, together with the D2-method proposed by Dongarra, Straughan & Walker (1996). Introducing the variables $\xi^{(1)} = (\mathrm{d}^2/\mathrm{d}y^2 - k^2)\phi^{(1)}$, $\xi^{(2)} = (\mathrm{d}^2/\mathrm{d}y^2 - k^2)\phi^{(2)}$, we can write the system of equations in the following form (see Appendix B):

$$\left(\frac{\mathrm{d}^2}{\mathrm{d}y^2} - k^2\right)\phi^{(1)} - \xi^{(1)} = 0,$$

$$\left(\frac{\mathrm{d}^2}{\mathrm{d}y^2} - k^2\right)\xi^{(1)} - \mathrm{i}kRe_1 U^{(1)}\xi^{(1)} + 2\mathrm{i}kRe_1 A_1\phi^{(1)} = -c\mathrm{i}kRe_1\xi^{(1)},$$

$$\left(\frac{\mathrm{d}^2}{\mathrm{d}y^2} - k^2\right)\phi^{(2)} - \xi^{(2)} = 0,$$

$$\left(\frac{\mathrm{d}^2}{\mathrm{d}y^2} - k^2\right)\xi^{(2)} - \mathrm{i}kRe_2 U^{(2)}\xi^{(2)} + 2\mathrm{i}kRe_2 A_2\phi^{(2)} = -c\mathrm{i}kRe_2\xi^{(2)}.$$

The computational domain is then mapped to $(-1, 1)$ for each fluid layer by the transformation

$$z = -2y - 1, \quad -1 \leqslant y \leqslant 0,$$
$$z = \frac{2}{n}y - 1, \quad 0 \leqslant y \leqslant n,$$

where $z = -1$ corresponds to the interface between the two fluids. The four functions $\phi^{(1)}$, $\xi^{(1)}$, $\phi^{(2)}$, $\xi^{(2)}$ are then expanded in series of Chebyshev polynomials $T_n(z)$. For N Chebyshev polynomials, we solve for the eigenvalues of a $4N \times 4N$ matrix. The continuity of the tangential and normal velocity components, and the continuity of

the tangential and normal stresses at the interface then take the form

$$\phi^{(1)} = \phi^{(2)}, \tag{4.1}$$

$$\frac{\mathrm{d}\phi^{(1)}}{\mathrm{d}z} + \frac{1}{n}\frac{\mathrm{d}\phi^{(2)}}{\mathrm{d}z} + \frac{a_1(1-\mu)}{2\mu}\hat{s} = 0, \tag{4.2}$$

$$2k^2\phi^{(1)} + \xi^{(1)} - 2k^2\mu\phi^{(2)} - \mu\xi^{(2)} + \mathrm{i}kRe_1E_bQ_T\hat{s} = 0, \tag{4.3}$$

$$-2k^2\frac{\mathrm{d}\phi^{(1)}}{\mathrm{d}z} + \frac{\mathrm{d}\xi^{(1)}}{\mathrm{d}z} - 2k^2\frac{\mu}{n}\frac{\mathrm{d}\phi^{(2)}}{\mathrm{d}z} + \frac{\mu}{n}\frac{\mathrm{d}\xi^{(2)}}{\mathrm{d}z} + \tfrac{1}{2}\mathrm{i}kRe_1E_bQ_N\hat{s} = 0. \tag{4.4}$$

The interfacial amplitude $\hat{s}$ in (4.2)–(4.4) is given by $\hat{s} = \phi^{(1)}(-1)/(c-1)$. When $\mu \neq 1$ and $a_1 \neq 0$, the amplitude of the interface $\hat{s}$ in (4.3)–(4.4) is given by $\hat{s} = -(\mathrm{d}\phi^{(1)}/\mathrm{d}z_1 + (1/n)(\mathrm{d}\phi^{(2)}/\mathrm{d}z_2)(2\mu/a_1(1-\mu))$. The eight boundary conditions are placed in the $j(N-1)$-th and jN-th ($j = 1, 2, 3, 4$) rows, as suggested by Dongarra *et al.* (1996).

Our computational code was verified by running the particular cases $Q_T = 0$ and $Q_N = 0$, and comparing with the results of Orszag (1971), Renardy (1985), Yiantsios & Higgins (1988), Hooper (1989) and Dongarra *et al.* (1996). In addition, since to our knowledge no EHD stability calculations have been reported in the literature so far, we used the long-wave results of the previous section to verify the code. We focus, first, on the effect of the electric field ($E_b \neq 0$) and the viscosity difference (viscosity stratification) on the stability of the flow, and therefore impose the same density $\rho = 1$ for the two fluids. The Reynolds number referred to in the computations is that of the lower fluid, Re_1. Finally, we note that the present method has been used in the absence of electric fields by Nagata (1990), who examined nonlinear effects and the bifurcation from infinity for plane Couette flow.

4.1. *Neutrally stable modes for* $\mu = 1$ *and* $\mu = n^2$

As we mentioned earlier, for Poiseuille flow there exist neutrally stable modes when $\mu = 1$ and $\mu = n^2$. These neutrally stable modes show that the viscous tangential shear stress vanishes at the interface between the two fluids, and our model for leaky dielectrics does not hold since the electrical tangential shear stress can no longer be balanced. However, our model for perfect dielectrics in the case where $\varepsilon = \sigma$ is still valid, since perfect dielectrics do not induce any electrical tangential shear stress. From the long-wave linear stability analysis, we know that the presence of the electric field in the case of perfect dielectrics always makes the flow unstable. We now present numerical results for all wavenumbers.

We first study one-fluid Poiseuille flow in a channel with an electric interface at the midplane of the channel, such that $\mu = 1$, $n = 1$ but $\sigma \neq 1$ and $\varepsilon \neq 1$, in which case the interface is due to the difference of permittivities and conductivities between the two fluids. It is well known that for one-fluid Poiseuille flow in a channel without an electric field, the critical Reynolds number for the onset of instability is about $Re_1 = 5772$. Although at higher Reynolds numbers, the instability is driven by the shear mode instead of the interfacial mode, and the long-wave stability analysis can no longer explain the instability mechanism, it is still interesting to investigate how the electric field alters the stability properties at high Reynolds numbers. Figure 6 shows the results of our computations using the electrical parameters $\varepsilon = \sigma = 4$, $E_b = 1$, and shows that the flow is unstable for all the Reynolds numbers we computed (the highest value being $Re_1 = 10^4$). We observe here that the flow is unstable for all Reynolds numbers presented; figures 6(*a*) to 6(*c*) show the most unstable eigenvalue c_i, the corresponding most unstable wavenumber k and the most unstable growth rate c_ik.

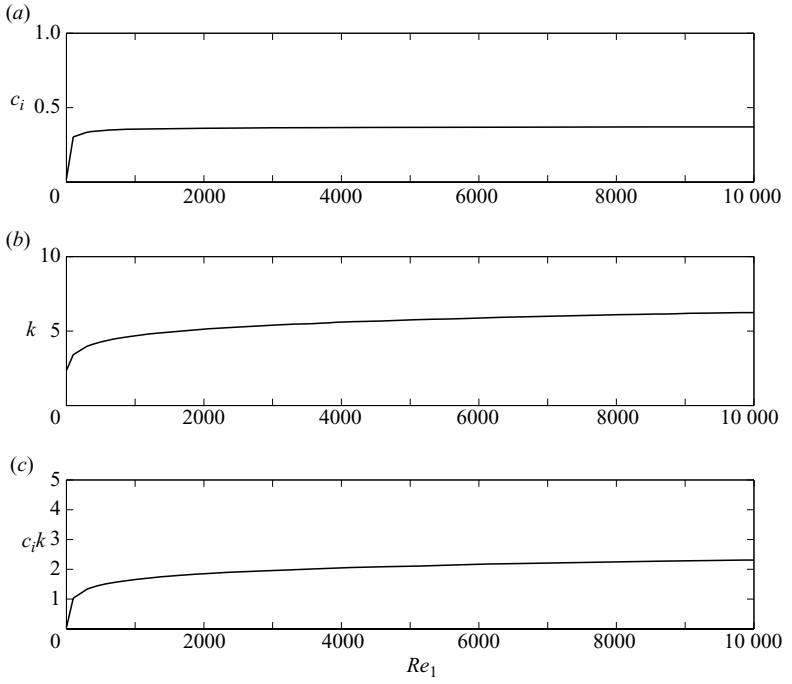

FIGURE 6. Impact of the electric field on the neutrally stable mode for a perfect dielectric in the case of a one-fluid Poiseuille flow with an initial electrical interface in the midplane of the channel. For $\mu = 1$, $n = 1$ and $\rho = 1$, the flow is unstable under the action of the electric field for $Re_1 \leqslant 10^4$ with $\varepsilon = 4$, $\sigma = 4$, and $E_b = 1$. (*a*) Most unstable mode c_i *vs.* Re_1; (*b*) wavenumber k of the most unstable mode *vs.* Re_1; (*c*) corresponding growth rate c_ik *vs.* Re_1.

Next, we consider the case when the two fluids have the same viscosity ($\mu = 1$), but different initial heights. We choose the value $n = 5$ and the electrical parameters $\varepsilon = \sigma = 4$, $E_b = 1$. Figure 7 shows that the flow is unstable for Reynolds numbers as large as 10^4. Figures 7(*a*) to 7(*c*) show the most unstable eigenvalue c_i, the corresponding wavenumber k and the most unstable growth rate c_ik, respectively.

Finally, we study the case where the two fluids are related by $\mu = n^2$. This is another case which supports neutrally stable modes in the absence of an electric field. In Figure 8, we show results for $\mu = 25$, $n = 5$, $\varepsilon = \sigma = 4$ and $E_b = 1$. The flow is again unstable for all computed Reynolds numbers. We observe that an electric field in the case of perfect dielectrics always has a destabilizing effect. This conclusion was established analytically using the long-wave theory, and our computations indicate that it can be extended to all wavenumbers. The result is of interest in practical applications such as microfluidics, where mixing between two fluids is often desired and should be realized in the case of perfect dielectrics, at least.

4.2. *Two-fluid Poiseuille flow*

We turn next to the more general case of a two-fluid Poiseuille flow where the two fluids have different viscosities ($\mu \neq 1$). The two-fluid Poiseuille flow in a channel in the absence of electric field ($E_b = 0$) is well documented (Yiantsios & Higgins 1988; Hooper 1989), and we study the influence of the addition of the electric field on the flow stability for arbitrary wavenumbers. When $E_b = 0$, and surface tension is neglected, it has been established (Yiantsios & Higgins 1988; Hooper 1989) that the

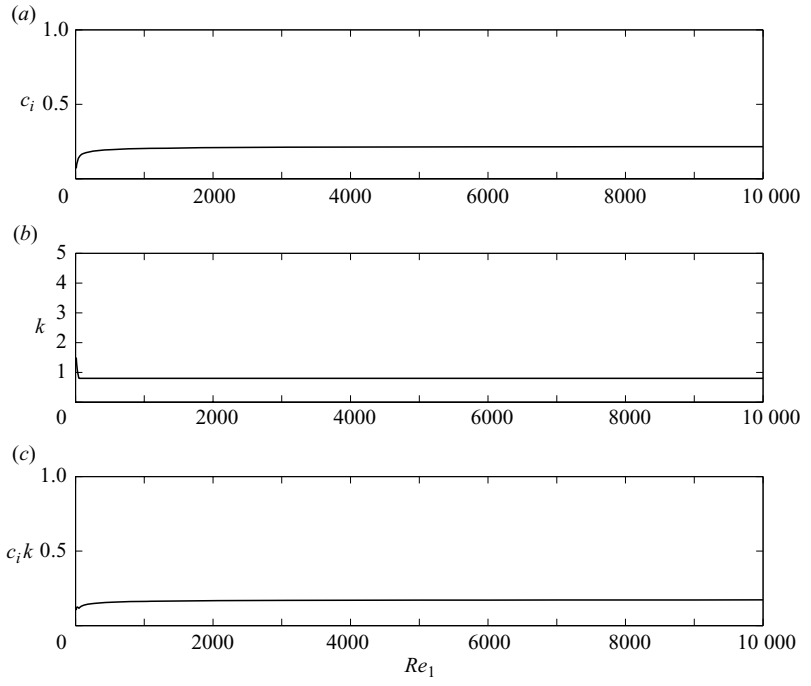

FIGURE 7. Impact of the electric field on the neutrally stable mode for a perfect dielectric in the case of a two-fluid Poiseuille flow with the same viscosity for the two fluids. For the parameter values $\mu = 1$, $n = 5$, $\rho = 1$, the flow is unstable under the action of the electric field for $Re_1 \leqslant 10^4$ with $\varepsilon = 4$, $\sigma = 4$ and $E_b = 1$. (*a*) Most unstable mode c_i *vs.* Re_1; (*b*) wavenumber k of the most unstable mode *vs.* Re_1; (*c*) corresponding growth rate $c_i k$ *vs.* Re_1.

stability depends on the particular values of the viscosity ratio μ and the layer depth ratio n. Recall that the long-wave analysis predicts the location of the stable and unstable domains in the (μ, n)-plane (figure 9). We choose the configuration having $\mu = 2$ and $n = 0.8$, which is unstable in the long-wave regime (figure 9). However, when the electric field is turned on, the long-wave stability depends on the choice of the permittivity and conductivity ratios, ε and σ. Thus, an unstable flow can become stable or more unstable, while a stable flow can become unstable or more stable.

Figure 10 shows the comparison of the most unstable (or least stable) mode c_i as a function of wavenumber k for this flow configuration obtained from both the spectral method computation and the long-wave result (3.21) under the action of the electric field. In all three cases, the long-wave theory describes the stability characteristics very well for values of k as large as 0.3, approximately. Figure 10(*b*) and 10(*c*) show calculations for non-zero E_b. The results in figure 10(*b*) correspond to $\sigma = 4$, $\varepsilon = 5$, $E_b = 0.5$, which according to the long-wave theory enhances the instability. This is indeed the case, as a comparison between figures 10(*a*) and 10(*b*) shows. Furthermore, this instability enhancement persists for larger values of k, as shown in the figure. The parameters in figure 10(*c*) are $\sigma = 2$, $\varepsilon = 10$, $E_b = 0.5$, which are values, at which, according to the long-wave theory, the flow should be fully stable. This stabilization is again observed to persist to order-one values of k also. It can be concluded, therefore, that the long-wave analysis is valuable in establishing the qualitative behaviour of the spectrum.

Figure 11 presents further details of the numerical results for the parameters $\mu = 2$, $n = 0.8$. We present the results up to wavenumbers $k = 20$, for various values of

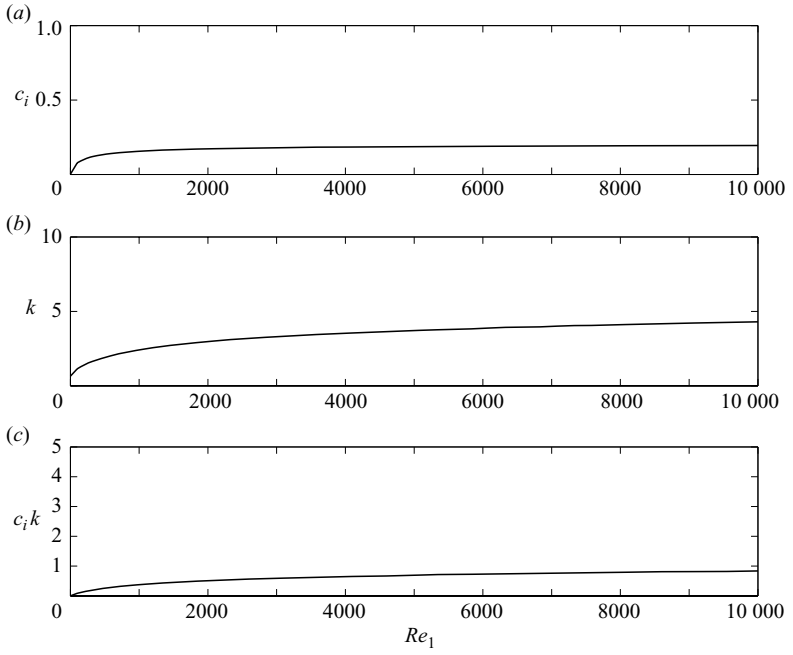

FIGURE 8. Impact of the electric field on the neutrally stable mode in the case of perfect dielectrics for a two-fluid Poiseuille flow with two fluids of different viscosities. For $\mu = 25$, $n = 5$, $\rho = 1$, the flow is unstable under the action of the electric field for Reynolds numbers such as $Re_1 \leqslant 10000$ with $\varepsilon = 4$, $\sigma = 4$, and $E_b = 1$. (*a*) Most unstable mode c_i *vs.* Re_1; (*b*) wavenumber k of the most unstable mode *vs.* Re_1; (*c*) corresponding growth rate $c_i k$ *vs.* Re_1.

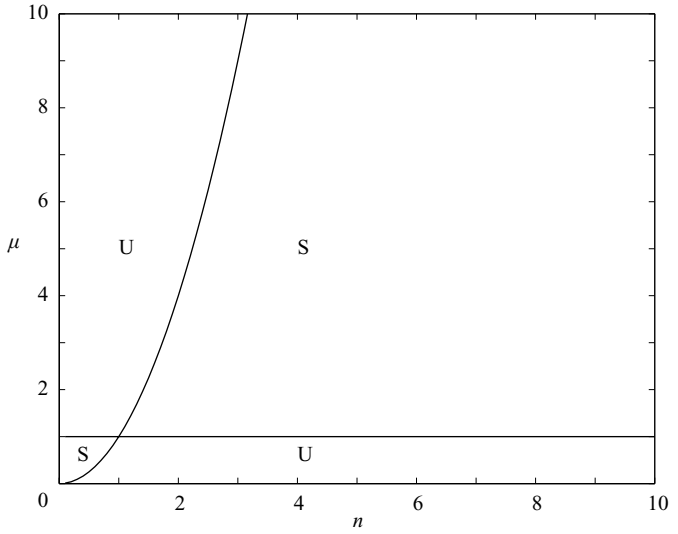

FIGURE 9. Long-wave analysis for Poiseuille flow without electric field: stable and unstable domains in the (μ, n)-plane.

the electrical parameter E_b. In figure 11(*a*) to 11(*c*), we show that the flow can be completely stabilized with $\sigma = 2$ and $\varepsilon = 10$ as E_b increases; figure 11(*a*) displays the most unstable (or least stable) mode c_i for $E_b = 0, 0.1, 0.5$; figure 11(*b*) shows the growth rate $c_i k$ for $E_b = 0, 0.1, 0.5$. Here, we see that the growth rate is almost

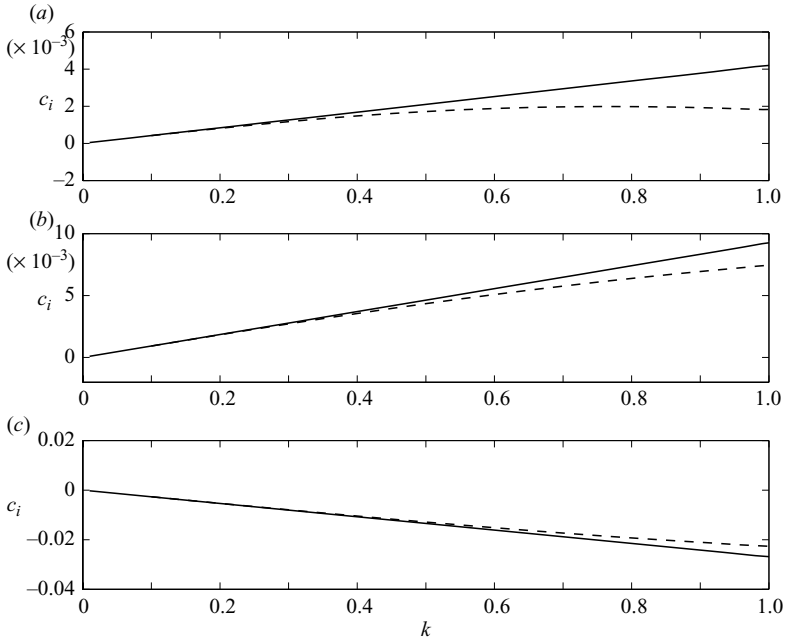

FIGURE 10. Two-fluid Poiseuille flow for the parameter values $\mu = 2$, $n = 0.8$, $Re_1 = 1$ and $\rho = 1$. Comparison of eigenvalues from the long-wave analysis (solid line) and the spectral method computation (dashed line). (*a*) $E_b = 0$, the flow is unstable for long waves without electric field; (*b*) $E_b = 0.5$, $\sigma = 4$, $\varepsilon = 5$, the flow becomes more unstable under the action of the electric field; (*c*) $E_b = 0.5$, $\sigma = 2$, $\varepsilon = 10$, the flow becomes stable under the action of the electric field.

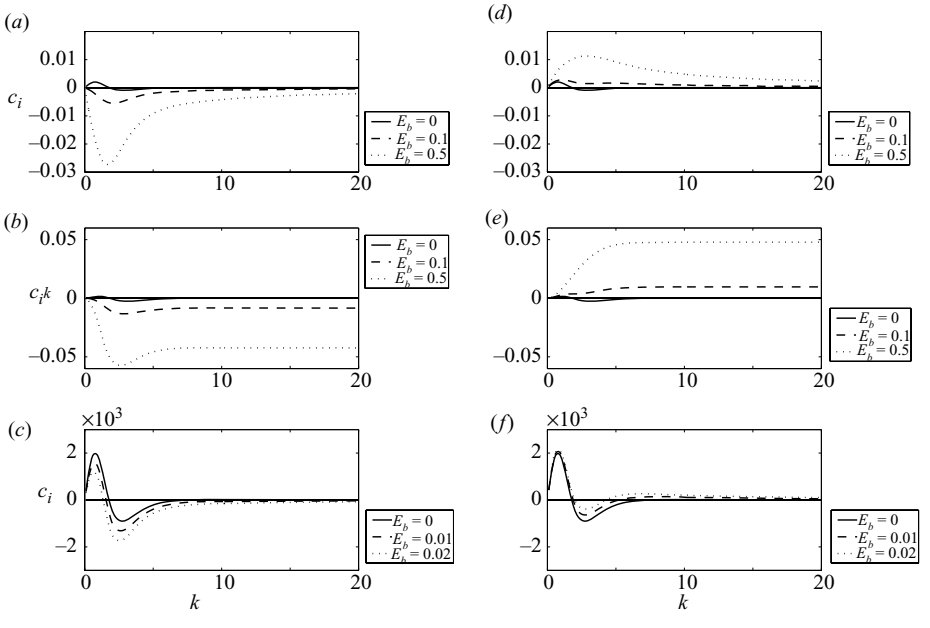

FIGURE 11. Two-fluid Poiseuille flow for the parameter values $\mu = 2$, $n = 0.8$, $Re_1 = 1$ and $\rho = 1$: details of the flow stability under the action of the electric field for different values of E_b. Without the electric field, the flow is unstable in the long-wave regime. (*a*)–(*c*) The flow becomes stable for $\varepsilon = 10$, $\sigma = 2$; (*d*)–(*f*) the flow becomes more unstable for $\varepsilon = 5$, $\sigma = 4$.

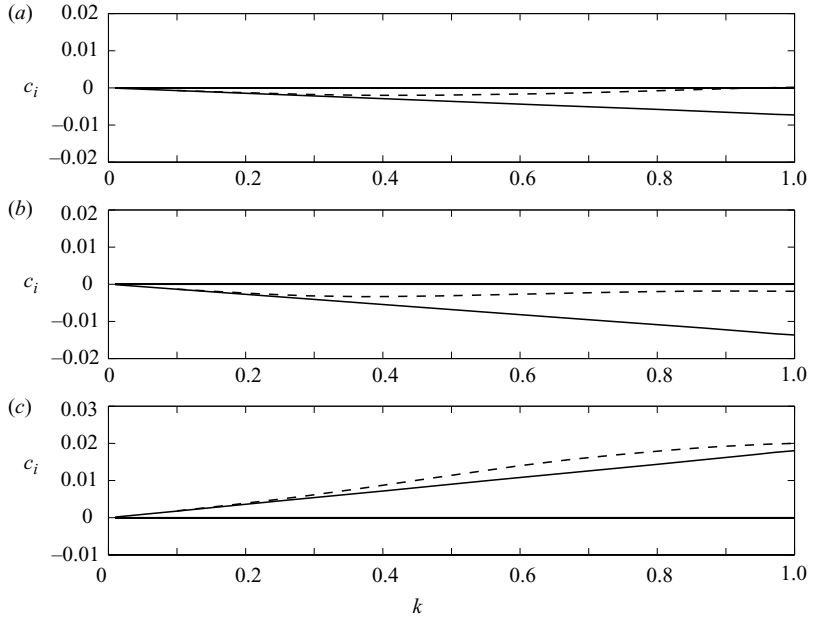

FIGURE 12. Two-fluid Poiseuille flow for the parameter values $\mu = 8$, $n = 3$, $Re_1 = 1$, $\rho = 1$; comparison of the eigenvalues obtained from the long-wave analysis (solid line) and the spectral method computation (dashed line). (*a*) $E_b = 0$, the flow is stable in the long-wave regime without the electric field; (*b*) $E_b = 0.5$, $\sigma = 2$, $\varepsilon = 10$, the flow becomes more stable under the action of the electric field; (*c*) $E_b = 0.5$, $\sigma = 4$, $\varepsilon = 5$, the flow becomes unstable under the action of the electric field.

constant when the wavenumber k is large (short-wave regime). Figure 11(*c*) shows the change of the most unstable mode in the initial stages of stabilization with E_b ranging from 0 to 0.02. In figure 11(*d*) to 11(*f*), we show that the flow can be completely destabilized when $\sigma = 4$ and $\varepsilon = 5$, as E_b increases; figure 11(*d*) presents the most unstable mode c_i for $E_b = 0, 0.1, 0.5$, and figure 11(*e*) displays the growth rate $c_i k$ for $E_b = 0, 0.1, 0.5$; finally, figure 11(*f*) shows the change in the most unstable mode in the initial stages of the destabilization with E_b ranging from 0 to 0.02.

In all cases presented, surface tension is absent. Short-wave instabilities (e.g. in figure 11*e*) exhibit a high-wavenumber cutoff when small amounts of surface tension are present – see later for a quantification of this observation.

In figures 12 and 13, we present results analogous to those in figures 10 and 11, but for the case where $\mu = 8$, $n = 3$. According to figure 9, this point is in the stable region (upper right domain marked S) as opposed to the previous set of results which are initially in the unstable regime. The results illustrate that the flow can become more stable (see figure 12(*b*) for $\sigma = 2$, $\varepsilon = 10$) or unstable (see figure 12(*c*) for $\sigma = 4$, $\varepsilon = 5$). Notice that the agreement with the asymptotic theory is again excellent. The characteristics at larger values of k are shown in figures 13. In figure 13(*a*), 13(*b*) and 13(*c*), we present the destabilization which results from increasing E_b for $\sigma = 4$ and $\varepsilon = 5$, while figure 13(*d*), 13(*e*) and 13(*f*) show the corresponding stabilization with increasing E_b for the parameters $\sigma = 2$, $\varepsilon = 10$. Surface tension is again absent and, if present, is responsible for providing large-wavenumber cutoffs.

Next, we study the effect of the electric field on neutral stability curves (NSC). We consider two types of NSC. The first type is determined with fixed Reynolds numbers

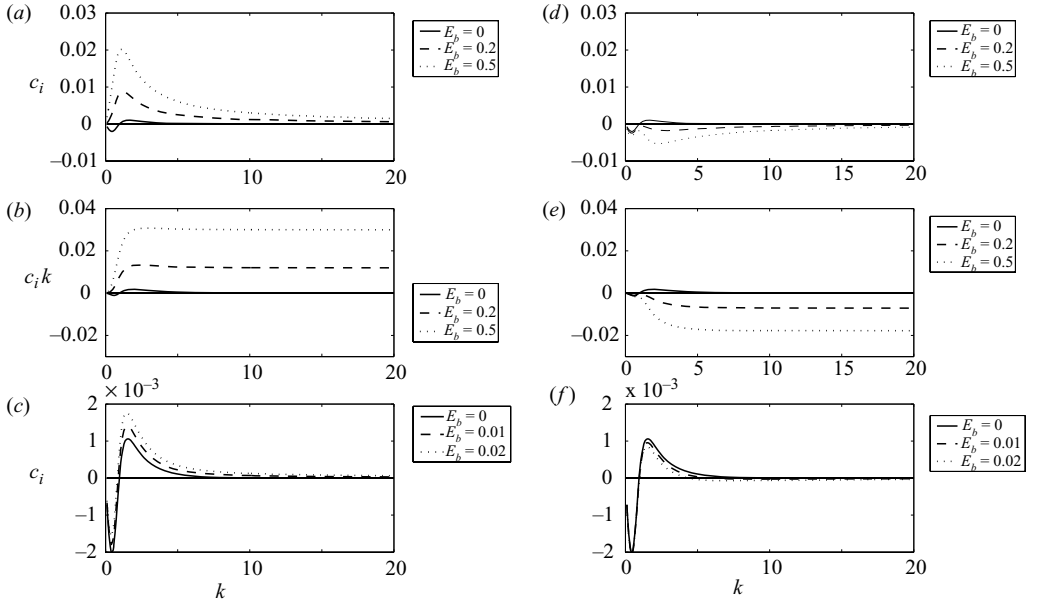

FIGURE 13. Two-fluid Poiseuille flow for the parameter values $\mu = 8$, $n = 3$, $Re_1 = 1$ and $\rho = 1$: details of the flow stability under the action of the electric field for different E_b values. Without the electric field, the flow is stable in the long-wave regime. (*a*)–(*c*) The flow becomes unstable for $\varepsilon = 5$, $\sigma = 4$; (*d*)–(*f*) the flow becomes more stable for $\varepsilon = 10$, $\sigma = 2$.

Re_1 and fixed viscosity ratios μ, and constructed in the (k, n)-plane, where n is the depth ratio of the two fluids. The second type is determined by fixing μ and n (i.e. the flow configuration), and is plotted in the (k, Re_1)-plane. We discuss both types of NSC under the influence of the electric field.

Figure 14 show, the effect of the electric field on the NSC of the first type for fixed parameter values $\mu = 2$ and $Re_1 = 1$. As already established, the stability depends on the specific values of σ and ε, and structurally different NSCs are expected for different pairs (σ, ε). As discussed earlier, in the framework of the linearized EHD equations, the case $\varepsilon = \sigma^2$ is a particular example where the electrical normal stress at the interface vanishes while the electrical tangential stress does not. Furthermore, the electrical normal stress acts in different directions across the interface for $\varepsilon > \sigma^2$ and $\varepsilon < \sigma^2$. We now present results corresponding to the following situations under relatively small electric fields, $E_b = 0.1$. Figure 14(*a*) reports the NSC without electric field $E_b = 0$, which was discussed in Hooper (1989); here, we see that $n = \sqrt{2}$ is a neutral stable line. Figure 14(*b*) shows the NSC when the electric field is applied with $\sigma = 4$ and $\varepsilon = 15$ ($\varepsilon < \sigma^2$); qualitatively, for $n < \sqrt{2}$, the NSC becomes a closed curve demarcating an isolated island of stability in a surrounding domain of instability and $n = \sqrt{2}$ is no longer a neutral stability line; when $n > \sqrt{2}$, the NSC has another separated branch enclosing a stable region (figure 14*b*). Figure 14(*c*) shows the NSC for $\sigma = 4$, $\varepsilon = 16$ ($\varepsilon = \sigma^2$); note that the NSC now evolves into two separated branches for $n < \sqrt{2}$ and $n > \sqrt{2}$ while $n = \sqrt{2}$ is still a neutral stability line for roughly $k \geqslant 1$ (this NSC is similar to that corresponding to $E_b = 0$). Figure 14(*d*) presents the NSC for $\sigma = 4$, $\varepsilon = 17$ ($\varepsilon > \sigma^2$); here, $n = \sqrt{2}$ is no longer a neutral stability line, and the shape of the curve is notably different from that of figure 14(*b*) and 14(*c*) and has an interesting topology.

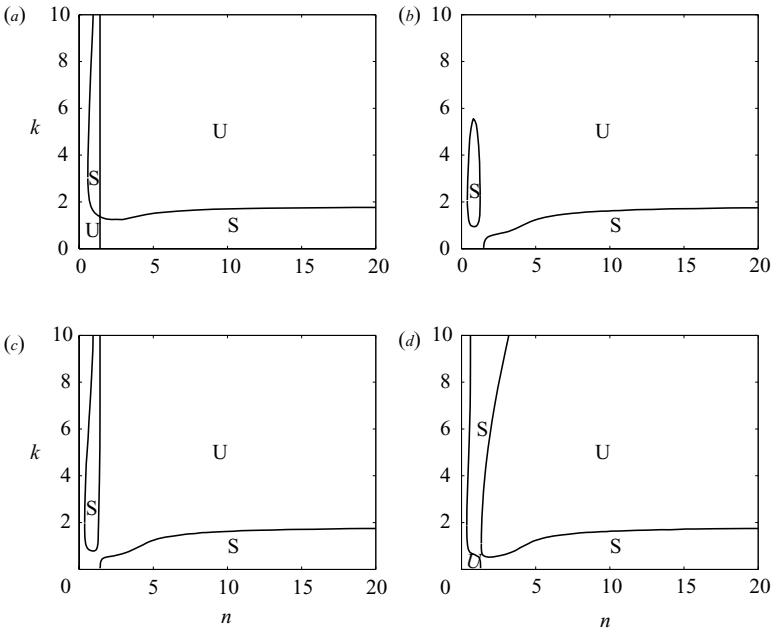

FIGURE 14. Two-fluid Poiseuille flow for the parameter values $\mu = 2$, $Re_1 = 1$ and $\rho = 1$: Neutral stability curve in the (k, n)-plane under the action of the electric field. (*a*) $E_b = 0$; (*b*) $E_b = 0.1$, $\sigma = 4$, $\varepsilon = 15$ ($\varepsilon < \sigma^2$); (*c*) $E_b = 0.1$, $\sigma = 4$, $\varepsilon = 16$ ($\varepsilon = \sigma^2$); (*d*) $E_b = 0.1$, $\sigma = 4$, $\varepsilon = 17$ ($\varepsilon > \sigma^2$).

It is worth mentioning that the shape of the NSC can be very complicated and typically it is difficult to predict how the curves change with the electric field. Next, we study the case having $\mu = 2$ and $Re_1 = 1$, but with an increased electric field such that $E_b = 1$. The NSCs in the (k, n)-plane are shown in figure 15 in three different domains of the electric field, i.e. $\varepsilon < \sigma^2$, $\varepsilon = \sigma^2$ and $\varepsilon > \sigma^2$. In all three cases, the curves for $n < 1$, approximately, are quite intricate (figures 15*a*, 15*c*, 15*e*). Figures 15(*a*) and 15(*b*) present results for $\sigma = 4$ and $\varepsilon = 15$ ($\varepsilon < \sigma^2$). We observe that for $n < \sqrt{2}$ in figure 15(*a*), the NSC consists of two separate branches and for small values of n (e.g. $n \approx 0.15$). As a result, the flow can be stable, unstable, then stable and finally unstable again when the wavenumber k increases from long to short wavenumbers, with n fixed. There is another branch at about $n > 8.5$ (figure 15*b*), and by comparing this branch with that of figure 14(*b*), we conclude that increasing the value of E_b from 0.1 to 1 makes the flow unstable in the region $\sqrt{2} < n \leqslant 8.5$. Figures 15(*c*) and 15(*d*) present the results for $\sigma = 4$ and $\varepsilon = 16$ ($\varepsilon = \sigma^2$); the NSC in this case has three branches for $n < \sqrt{2}$ as seen in figure 15(*c*), and $n = \sqrt{2}$ is still a neutral stable line for about $k > 5$ (short waves). Figures 15(*e*) and 15(*f*) depict results for $\sigma = 4$ and $\varepsilon = 17$ ($\varepsilon > \sigma^2$). Here, the NSC has two branches for $n > 1$ and for some certain values of n, e.g. $n = 10$, the flow is unstable, stable, then unstable and finally stable again when k increases from small to large wavenumbers. These numerical results at general values of k, imply that a sufficiently strong electric field can destabilize long waves which are otherwise stable for moderately large values of n (this is the so-called thin-layer effect as described in Chen (1995) in the absence of electric fields) – compare for example figures 14(*a*), 14(*d*) with figure 15(*f*). The complicated stability characteristics uncovered in the results of figure 15 indicate that caution must be exercised when applying long-wave theories valid for small k and hoping

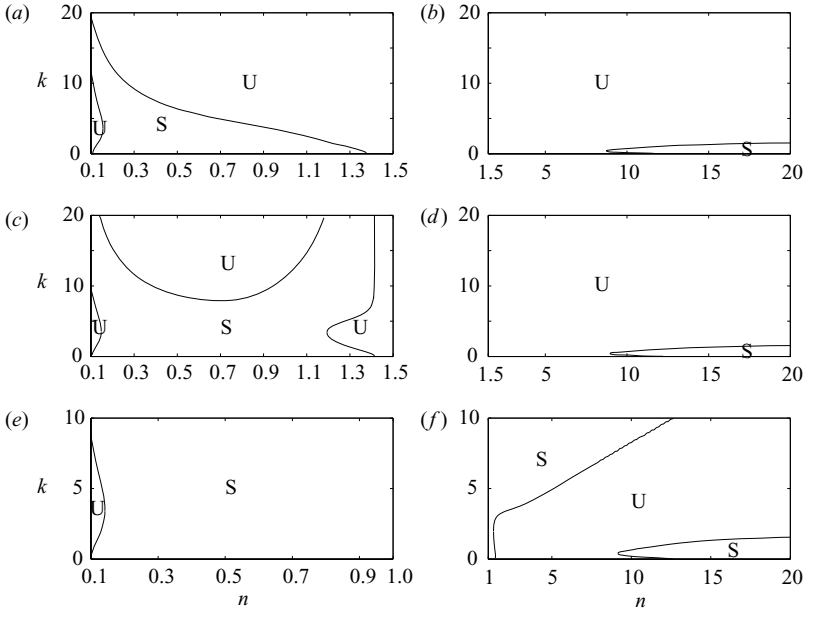

FIGURE 15. Two-fluid Poiseuille flow for the parameter values $\mu = 2$, $Re_1 = 1$, $\rho = 1$ and $E_b = 1$: neutral stability curve in the (k, n)-plane under the action of the electric field in various cases. (*a*) $\sigma = 4$, $\varepsilon = 15$ ($\varepsilon < \sigma^2$), $0.1 < n < 1.5$; (*b*) $\sigma = 4$, $\varepsilon = 15$ ($\varepsilon < \sigma^2$), $1.5 < n < 20$; (*c*) $\sigma = 4$, $\varepsilon = 16$ ($\varepsilon = \sigma^2$), $0.1 < n < 1.5$; (*d*) $\sigma = 4$, $\varepsilon = 16$ ($\varepsilon = \sigma^2$), $1.5 < n < 20$; (*e*) $\sigma = 4$, $\varepsilon = 17$ ($\varepsilon > \sigma^2$), $0.1 < n < 1$; (*f*) $\sigma = 4$, $\varepsilon = 17$ ($\varepsilon > \sigma^2$), $1 < n < 20$.

for the qualitative predictions to hold at larger k also. As an example, we consider $n = 10$ in figure 15(*f*). The flow is initially long-wave unstable, but as k is increased, we calculated a band of stability with relatively long waves; this then gives way to a band of instability and finally the flow becomes short-wave stable at sufficiently large k. The short-wave stability comes from the presence of an electric field (surface tension is absent throughout) – in fact, in the absence of an electric field, the flow is short-wave unstable for sufficiently large n (see figure 14*a*), and we can see that the electric field can be used to reverse such characteristics.

Figure 16 shows the effect of the electric field on the NSC in the (k, n)-plane for a large viscosity ratio $\mu = 20$, $E_b = 1$ and fixed Reynolds number $Re_1 = 1$. The NSC without electric field ($E_b = 0$) is shown in figure 16(*a*), showing that $n = \sqrt{20}$ is a neutral stable line. The effect of the electric field on the NSC in the (k, n)-plane is presented for $\sigma = 6$ in three cases: figure 16(*b*), $\varepsilon = 35$ ($\varepsilon < \sigma^2$); figure 16(*c*), $\varepsilon = 36$ ($\varepsilon = \sigma^2$); figure 16(*d*) $\varepsilon = 37$ ($\varepsilon > \sigma^2$). We see that the NSCs have shapes which are topologically similar to those corresponding to $\mu = 2$ and $E_b = 0.1$ in figure 14.

We now discuss (figure 17) the second type of neutral stability curves in the (k, Re_1)-plane for a specific flow configuration corresponding to fixed values of $\mu = 2$ and $n = 10$. The NSC without electric field ($E_b = 0$) has been calculated by Hooper (1989) up to Reynolds numbers of around $Re_1 = 600$. In figure 17(*a*), we confirm Hooper's results and extend them up to $Re_1 = 10^3$. An interfacial mode triggered by the difference in viscosities between the two fluids occurs for moderate Reynolds-number values (surface tension being absent). However, at about $Re_1 = 290$, a shear mode caused by the difference of shear velocities between the two fluids, is seen to appear and the two modes coexist for a certain range of Reynolds numbers. For the

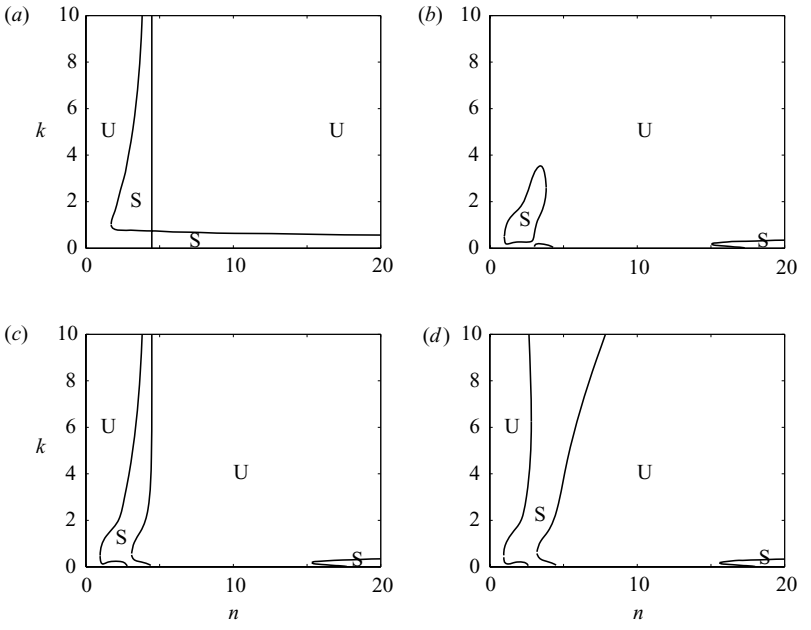

FIGURE 16. Two-fluid Poiseuille flow for the parameter values $\mu = 20$, $Re_1 = 1$, $\rho = 1$: neutral stability curve in the (k, n)-plane under the action of the electric field in various cases. (*a*) $E_b = 0$; (*b*) $E_b = 1$, $\sigma = 6$, $\varepsilon = 35$ ($\varepsilon < \sigma^2$); (*c*) $E_b = 1$, $\sigma = 6$, $\varepsilon = 36$ ($\varepsilon = \sigma^2$); (*d*) $E_b = 1$, $\sigma = 6$, $\varepsilon = 37$ ($\varepsilon > \sigma^2$).

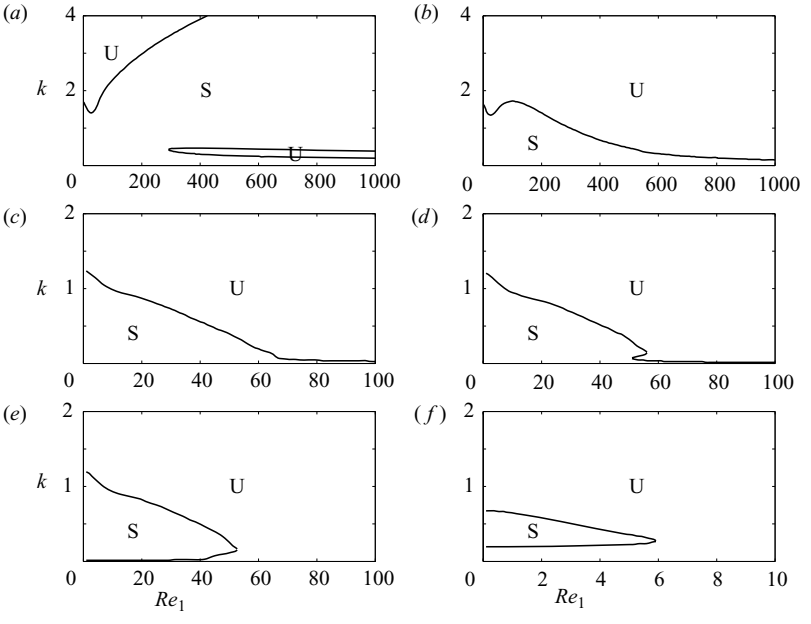

FIGURE 17. Two-fluid Poiseuille flow for the parameter values $n = 10$, $\mu = 2$ and $\rho = 1$, showing the changes in the neutral stability curve in the plane (k, Re_1) under the action of the electric field for $\sigma = 4$, $\varepsilon = 17$ and different E_b values. (*a*) $E_b = 0$, $Re_1 < 1000$; (*b*) $E_b = 0.1$, $Re_1 < 1000$; (*c*) $E_b = 0.53$, $Re_1 < 100$; (*d*) $E_b = 0.55$, $Re_1 < 100$; (*e*) $E_b = 0.56$, $Re_1 < 100$; (*f*) $E_b = 1$, $Re_1 < 10$.

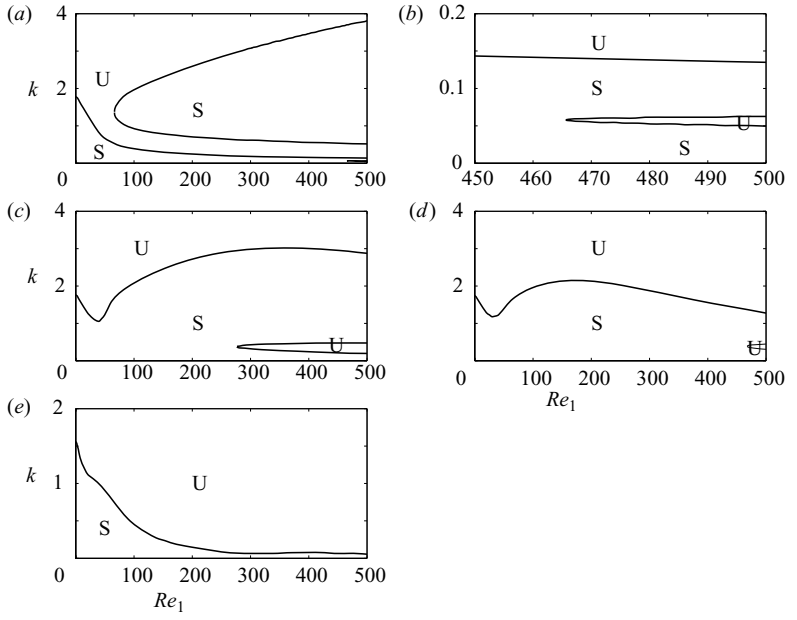

FIGURE 18. Two-fluid Poiseuille flow for the parameter values $n = 20$, $\mu = 2$ and $\rho = 1$. Neutral stability curve in the (k, Re_1)-plane under the action of the electric field for different E_b values for $\sigma = 4$, $\varepsilon = 17$. (*a*) $E_b = 0$, $Re_1 < 500$; (*b*) $E_b = 0$, $450 < Re_1 < 500$; (*c*) $E_b = 0.1$, $Re_1 < 500$; (*d*) $E_b = 0.2$, $Re_1 < 500$; (*f*) $E_b = 1$, $Re_1 < 500$.

one-fluid Poiseuille flow, the shear mode emerges at about $Re_1 = 5772$, and in the two-fluid cases studied here it can appear at much smaller Reynolds numbers. We also find that when the two modes co-exist, the interfacial mode dominates at short wavelengths (surface tension being absent), while the shear mode predominates at long wavelengths. Such stability characteristics are relatively clear, but they become more complex in the presence of an electric field. To illustrate this, we present results of a computation having $\sigma = 4$, $\varepsilon = 17$ and different values of E_b, as shown in figure 17(*b–f*) (these values of conductivity and permittivity ratios place the flow in the stable regime, $J_E < 0$, according to the long wave theory – see figure 5). Specifically, figure 17(*b*) shows that for $E_b = 0.1$, the shear mode disappears and the instability is dominated by the interfacial mode. The upper and lower branch structure typical of high-Reynolds-number instabilities in shear flows appears to be pushed to higher Reynolds numbers, which falls outside our computational range (our computations go as high as $Re_1 = 10^3$). At the same time, the interfacial mode loses stability and bends down to support a larger unstable domain (see figure 17*d*). In figures 17(*c*), 17(*d*), 17(*e*) and 17(*f*), the value of E_b is increased systematically and the overall finding is that the instability is enhanced. In particular, at a value of E_b between 0.55 and 0.56, the open branch that is indicated in figure 17(*b*) becomes closed and the island of stability it supports shrinks with increasing E_b - compare the neutral curves in going from figure 17(*c*) to 17(*f*) (the results show the effect of the electric field on the interfacial mode – the shear mode probably existing as well, but at a much larger value of Re_1). We found numerically that as Re_1 increases further, the island of stability shrinks and disappears completely at approximately $Re_1 = 6$.

Figure 18 shows the NSC for the case $\mu = 2$ and $n = 20$, where the upper layer is twice as thick as in the case of figure 17. Hooper (1989) presented the NSC without an electric field ($E_b = 0$) up to a Reynolds number of about $Re_1 = 130$ for these values

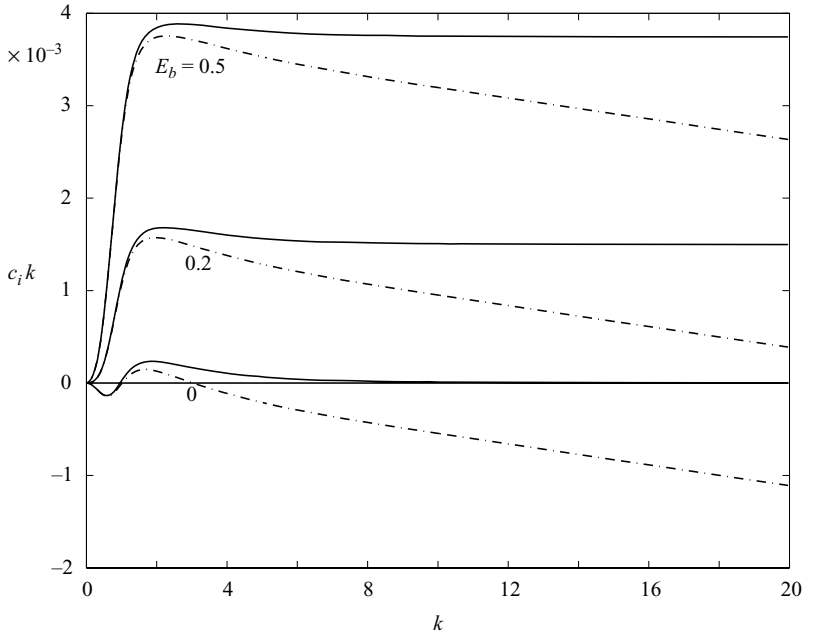

FIGURE 19. Two-fluid Poiseuille flow with the parameter values $n = 3$, $\mu = 8$, $\rho = 1$, $\sigma = 4$, $Re_1 = 1$ and $\varepsilon = 5$. Solid lines correspond to the results in the absence of surface tension, while dashed lines show the results when $T = 0.001$.

of μ and n. However, we have run our code up to $Re_1 = 500$ and detected another shear mode at about $Re_1 = 465$, as shown in figures 18(a) and 18(b). (The presence of two shear modes is an interesting characteristic of the two-fluid flow.) Figure 18(c) shows the neutral curves at the relatively small value of $E_b = 0.1$. The overall effect of the electric field in this case is to stabilize long waves and destabilize short waves. The two main branches discernible in figure 18(a) merge when $E_b = 1$ to produce a main upper branch above which the flow is unstable, and a loop consisting of an upper and lower branch inside which the flow is unstable – see figure 18(c). The second shear mode shown in the magnification (figure 18b), completely disappears when the field is turned on and most probably shifts to much higher Reynolds numbers. A further increase of E_b to a value of 0.2 (see figure 18d) enhances the trends noted above, namely, short waves are destabilized and long waves stabilized. This manifests itself by the lowering of the main upper branch and the shift to higher Reynolds numbers of the upper and lower branch loops which supports instability for a narrow range of wavenumbers (the nose of the loop is only just present at $E_b = 0.2$ as seen in the lower right-hand part of figure 18d). A further increase to $E_b = 1$ (see figure 18e) reinforces the destabilization and for the range of parameters used in our computations, the main upper branch is the only feature left, dividing the (Re_1, k)-plane into an upper unstable domain and a lower stable one, stability being possible only for sufficiently long waves.

Thus far, we have investigated the role of the electric field on the interfacial instability in the absence of surface tension. Surface tension acts to stabilize sufficiently short waves and we provide representative results of its effect on the instability of the present problem. In figures 19 and 20, we show the effect of surface tension on the results of figure 13. The value of the surface tension parameter is $T = 0.001$. Figure 19 corresponds to the modifications of figure 13(c) and shows growth rates

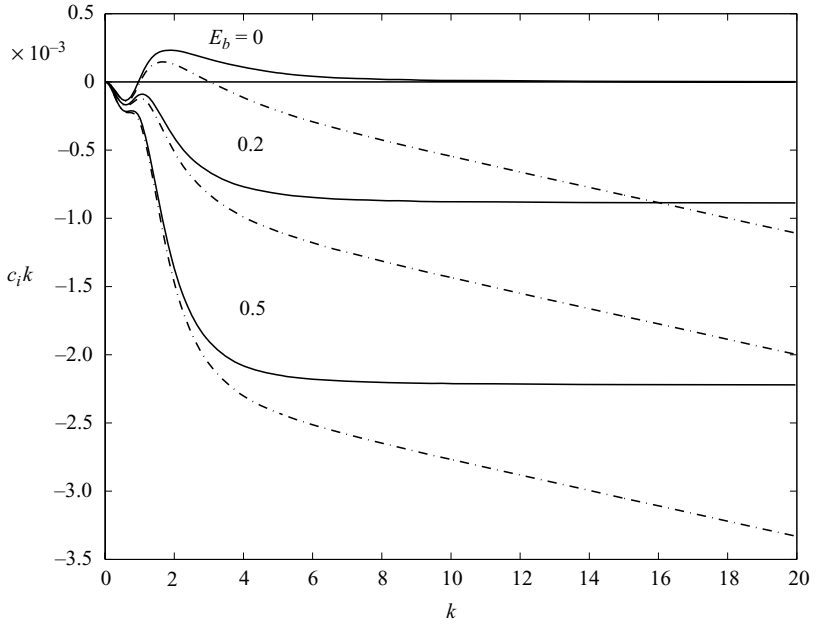

FIGURE 20. Two-fluid Poiseuille flow for the parameters $n = 3$, $\mu = 8$, $\rho = 1$, $\sigma = 2$ and $\varepsilon = 10$. Solid lines correspond to the results in the absence of surface tension, while dashed lines show the results when $T = 0.001$.

versus wavenumber for $n = 3$, $\mu = 8$, $Re_1 = 1$, $\rho = 1$, $\sigma = 4$ and $\varepsilon = 5$ (for this set of parameters, the electric field is destabilizing – see earlier remark). It is seen that the presence of surface tension modifies the short-wave behaviour (large k) and provides a cutoff value (which increases with E_b) above which the waves are damped. For longer waves (in fact for $k < 1$, approximately), the effect of surface tension is not significant. Similar findings are established from the computations presented in figure 20 which adds surface tension to the results of figure 13(d) for $n = 3$, $\mu = 8$, $Re_1 = 1$, $\rho = 1$, $\sigma = 2$ and $\varepsilon = 10$ (the electric field is now stabilizing). As observed from the figure, surface tension provides a wavenumber cutoff at a value of $k \approx 3$ for the $E_b = 0$ results, and enhances the damping of short waves according to $c_i k \sim -k$ for $k \gg 1$ (this asymptotic behaviour is generic in the presence of surface tension in the present problem, and for brevity it is not analysed further). In addition, surface tension reduces growth rates of the most unstable (or least stable) waves, as seen from the results in figures 19 and 20.

5. Conclusions

In this work, we have studied the linear stability of two conducting viscous fluids bounded between channel walls and subjected to an electric field normal to the fluid interface. We have studied the general situation where the fluids are leaky dielectrics, which supports surface charges at the interface, as well as the situation where the fluids can be modelled as perfect dielectrics, which was considered as a special case in our study. The two fluids can have different viscosities, densities, permittivities and, more importantly, different finite conductivities. As a consequence, the electric field can cause an electrical tangential shear stress at the interface.

We have performed the long-wave linear stability analysis within the general Orr–Sommerfeld framework, considering that the base flow can be either Couette or

Poiseuille flow. We have then derived a general expression for the eigenvalue for the wave speed, c, which depends on the ratio of permittivities ε, ratio of conductivities σ, ratio of viscosities μ, and ratio of initial depths n of the two fluid layers.

For perfect dielectrics, where there are no surface charges at the interface (EH-Ip), or for a perfectly conducting interface where the conductivity of one fluid is much higher than that of the other fluid (EH-If), there is only a normal polarization force and no electrical tangential shear stress induced by the electric field at the interface. In this case, the electric field always has a destabilizing effect for both types of base flow investigated (Couette and Poiseuille flow), independently of the particular value of the ratio of permittivities ε. This confirms the results available in the literature (Melcher 1963; Mohamed *et al.* 1995). This result has great significance for practical applications, such as those where mixing is highly sought, e.g. in microfluidic systems.

On the other hand, for leaky dielectrics where the interface admits surface charges due to the finite conductivity of the two fluids, we have shown that the electric field can have either a destabilizing or a destabilizing effect, depending on the ratio of permittivities ε and ratio of conductivities σ between the two fluids. Since for both Couette and Poiseuille flows, there always exist unstable modes due to viscosity stratification, it is possible to stabilize the system by using an electric field.

We have also addressed the stability problem for all wavenumbers using numerical computations based on the Chebyshev spectral method. The long-wave dispersion relation earlier derived analytically was confirmed numerically in the absence of surface tension. Numerical simulations also led to different shapes for the neutral stability curve (NSC) under the action of the electric field. One important result found here was that the electrical normal stress can vanish at the interface while the electrical tangential stress remains non-zero. Based on the different directions of the electrical normal stress at the interface ($\varepsilon = \sigma^2$, $\varepsilon < \sigma^2$ or $\varepsilon > \sigma^2$), the NSC can take different forms.

Finally, we consider surface-tension effects. As pointed out by a referee, surface tension coupled with the thin-layer effect (see § 1), can completely stabilize a two-layer system at low Reynolds numbers. We can use our present results to speculate judiciously on the effect of surface tension in the presence of electric fields. For example, figure 16(*a*) shows a long-wave stability with $E_b = 0$ at moderately large n, along with short-wave instability due to zero surface tension. Inclusion of surface tension may completely stabilize this region. Inspection of figure 16(*b*), indicates that inclusion of an electric field completely destabilizes the flow for a range of n; inclusion of surface tension would regularize the short-wave instability.

We gratefully acknowledge the support of the New Jersey Commission on Science and Technology through the New-Jersey Center for Micro-Flow Control under Award Numbers 01-2042-007-25 and 05-2042-014-30. The work of D. T. P. was supported by the National Science Foundation Grant DMS-0072228. O. O. was also partially supported by an NJIT Presidential Initiative Fellowship.

Appendix A

The non-dimensional system of equations reads

$$\nabla \cdot \boldsymbol{u}^{(i)} = 0, \quad i = 1, 2, \tag{A 1}$$

$$\frac{\partial u^{(1)}}{\partial t} + \left(\boldsymbol{u}^{(1)} \cdot \nabla\right) u^{(1)} = -\frac{\partial p^{(1)}}{\partial x} + \frac{1}{Re_1} \nabla^2 u^{(1)}, \tag{A 2}$$

$$\frac{\partial v^{(1)}}{\partial t} + \left(\boldsymbol{u}^{(1)} \cdot \nabla\right) v^{(1)} = -\frac{\partial p^{(1)}}{\partial y} - \frac{1}{F} + \frac{1}{Re_1}\nabla^2 v^{(1)}, \tag{A 3}$$

$$\frac{\partial u^{(2)}}{\partial t} + \left(\boldsymbol{u}^{(2)} \cdot \nabla\right) u^{(2)} = -\frac{1}{\rho}\frac{\partial p^{(2)}}{\partial x} + \frac{1}{Re_2}\nabla^2 u^{(2)}, \tag{A 4}$$

$$\frac{\partial v^{(2)}}{\partial t} + \left(\boldsymbol{u}^{(2)} \cdot \nabla\right) v^{(2)} = -\frac{1}{\rho}\frac{\partial p^{(2)}}{\partial y} - \frac{1}{F} + \frac{1}{Re_2}\nabla^2 v^{(2)}, \tag{A 5}$$

$$u^{(1)}(-\eta_1) = 0, \quad v^{(1)}(-\eta_1) = 0, \tag{A 6}$$

$$u^{(2)}(\eta_2) = 1, \quad v^{(2)}(\eta_2) = 0, \tag{A 7}$$

$$S_t + S_x u^{(i)} = v^{(i)} \quad \text{on} \quad y = S(x,t), \tag{A 8}$$

$$V^{(i)}_{xx} + V^{(i)}_{yy} = 0, \quad i = 1, 2, \tag{A 9}$$

$$V^{(1)}(-\eta_1) = 0, \tag{A 10}$$

$$V^{(2)}(\eta_2) = 1, \tag{A 11}$$

$$S_x [V_y]^1_2 + [V_x]^1_2 = 0 \quad \text{on} \quad y = S(x,t), \tag{A 12}$$

$$S_x [\sigma V_x]^1_2 = [\sigma V_y]^1_2 \quad \text{on} \quad y = S(x,t), \tag{A 13}$$

$$u^{(1)} = u^{(2)} \quad \text{on} \quad y = S(x,t), \tag{A 14}$$

$$v^{(1)} = v^{(2)} \quad \text{on} \quad y = S(x,t), \tag{A 15}$$

$$\begin{aligned} &2S_x \left[\frac{1}{Re_1}\left(\frac{\partial v^{(1)}}{\partial y} - \frac{\partial u^{(1)}}{\partial x}\right) - \frac{\rho}{Re_2}\left(\frac{\partial v^{(2)}}{\partial y} - \frac{\partial u^{(2)}}{\partial x}\right)\right] \\ &\quad \times \left(1 - S_x^2\right)\left[\frac{1}{Re_1}\left(\frac{\partial u^{(1)}}{\partial y} + \frac{\partial v^{(1)}}{\partial x}\right) - \frac{\rho}{Re_2}\left(\frac{\partial u^{(2)}}{\partial y} + \frac{\partial v^{(2)}}{\partial x}\right)\right] \\ &\quad + S_x E_b\left([M_{22}]^1_2 - [M_{11}]^1_2\right) + \left(1 - S_x^2\right) E_b [M_{12}]^1_2 = 0 \quad \text{on} \quad y = S(x,t), \end{aligned} \tag{A 16}$$

$$\begin{aligned} &p_2 - p_1 + \frac{2}{Re_1\left(1 + S_x^2\right)}\left[S_x^2\frac{\partial u^{(1)}}{\partial x} - S_x\left(\frac{\partial u^{(1)}}{\partial y} + \frac{\partial v^{(1)}}{\partial x}\right) + \frac{\partial v^{(1)}}{\partial y}\right] - \frac{2\rho}{Re_2\left(1 + S_x^2\right)} \\ &\quad \times \left[S_x^2\frac{\partial u^{(2)}}{\partial x} - S_x\left(\frac{\partial u^{(2)}}{\partial y} + \frac{\partial v^{(2)}}{\partial x}\right) + \frac{\partial v^{(2)}}{\partial y}\right] + \left(S_x^2 [M_{11}]^1_2 - 2S_x [M_{12}]^1_2 + [M_{22}]^1_2\right) \\ &\quad \times \frac{E_b}{1 + S_x^2} - \frac{T S_{xx}}{\left(1 + S_x^2\right)^{\frac{3}{2}}} = 0 \quad \text{on } y = S(x,t), \end{aligned} \tag{A 17}$$

where

$$[M_{11}]^1_2 = \tfrac{1}{2}\left[\left(\chi_x^{(1)}\right)^2 - \left(\frac{\sigma}{\eta_2 + \sigma\eta_1} + \chi_y^{(1)}\right)^2\right] - \tfrac{1}{2}\varepsilon\left[\left(\chi_x^{(2)}\right)^2 - \left(\frac{1}{\eta_2 + \sigma\eta_1} + \chi_y^{(2)}\right)^2\right],$$

$$[M_{12}]^1_2 = \left[\chi_x^{(1)}\left(\frac{\sigma}{\eta_2 + \sigma\eta_1} + \chi_y^{(1)}\right) - \varepsilon\chi_x^{(2)}\left(\frac{1}{\eta_2 + \sigma\eta_1} + \chi_y^{(2)}\right)\right],$$

$$[M_{22}]^1_2 = -[M_{11}]^1_2.$$

Appendix B

The first-order problem can be written as

$$\frac{\mathrm{d}^4\phi_1^{(1)}}{\mathrm{d}y^4} = \mathrm{i}Re_1\left[\left(U^{(1)}-c_0\right)\frac{\mathrm{d}^2\phi_0^{(1)}}{\mathrm{d}y^2} - \phi_0^{(1)}\frac{\mathrm{d}^2U^{(1)}}{\mathrm{d}y^2}\right],$$

$$\frac{\mathrm{d}^4\phi_1^{(2)}}{\mathrm{d}y^4} = \mathrm{i}Re_2\left[\left(U^{(2)}-c_0\right)\frac{\mathrm{d}^2\phi_0^{(2)}}{\mathrm{d}y^2} - \phi_0^{(2)}\frac{\mathrm{d}^2U^{(2)}}{\mathrm{d}y^2}\right],$$

$$\phi_1^{(1)}(-\eta_1) = \frac{\mathrm{d}\phi_1^{(1)}}{\mathrm{d}y}(-\eta_1) = 0, \quad \phi_1^{(2)}(\eta_2) = \frac{\mathrm{d}\phi_1^{(2)}}{\mathrm{d}y}(\eta_2) = 0,$$

$$\frac{\mathrm{d}^2\phi_1^{(1)}}{\mathrm{d}y^2}(0) - \mu\frac{\mathrm{d}^2\phi_1^{(2)}}{\mathrm{d}y^2}(0) + \mathrm{i}Re_1E_bQ_T = 0,$$

$$\frac{\mathrm{d}^3\phi_1^{(1)}}{\mathrm{d}y^3}(0) - \mu\frac{\mathrm{d}^3\phi_1^{(2)}}{\mathrm{d}y^3}(0) + \mathrm{i}Re_1(\rho Q_0 - E_bQ_N) = 0,$$

$$\frac{\mathrm{d}\phi_1^{(1)}}{\mathrm{d}y}(0) - \frac{\mathrm{d}\phi_1^{(2)}}{\mathrm{d}y}(0) = -\frac{c_1\phi_0(0)}{(c_0-1)^2}(a_2-a_1),$$

where we have used the fact that $\hat{s} = \hat{s}_0 + k\hat{s}_1 + O(k^2)$, $\hat{s}_0 = \phi_0(0)/(c_0-1)$, $\hat{s}_1 = -c_1\phi_0(0)/(c_0-1)^2$, $\phi_0(0) = 1$. The terms Q_0, Q_T, Q_N can be simplified to lead to the following expressions: $Q_0 = ((\rho-1)/\rho F)(1/(c_0-1)) + (1/\rho-1)[(c_0-1)B_2 + a_2]$, $Q_T = \sigma(\sigma-\varepsilon)(\eta_1+\eta_2)/(\eta_2+\sigma\eta_1)^3$, $Q_N = (\sigma-1)(\varepsilon-\sigma^2)/(\eta_2+\sigma\eta_1)^3$. The solution to the first order then becomes

$$\phi_1^{(1)} = B_{11}y + C_{11}y^2 + D_{11}y^3 + H_1(y),$$

$$\phi_1^{(2)} = B_{12}y + C_{12}y^2 + D_{12}y^3 + H_2(y),$$

where $H_1(y)$, $H_2(y)$ are the particular solutions of the first order ODE problem given by

$$H_1(y) = \frac{A_1D_{01}}{210}y^7 + \frac{a_1D_{01}}{60}y^6 + \frac{a_1C_{01} - 3c_0'D_{01} - A_1B_{01}}{60}y^5 - \frac{c_0'C_{01} + A_1}{12}y^4,$$

$$H_2(y) = \frac{A_2D_{02}}{210}y^7 + \frac{a_2D_{02}}{60}y^6 + \frac{a_2C_{02} - 3c_0'D_{02} - A_2B_{02}}{60}y^5 - \frac{c_0'C_{02} + A_2}{12}y^4.$$

Here, $c_0' = c_0 - 1$, A_i, a_i come from the velocity profiles (2.16), (2.17), and the coefficients B_{0i}, C_{0i} and D_{0i} $(i = 1, 2)$ can be deduced from the leading-order solution. Since the constant factor of the eigenvalue is taken to be $\phi^{(1)}(0) = \phi^{(2)}(0) = \phi(0) = 1$, the constant term in the first-order solutions is chosen to be zero. The coefficients B_{1i}, C_{1i}, D_{1i} $(i = 1, 2)$ are solved from the first-order boundary conditions and the first-order eigenvalue takes the form

$$c_1 = \mathrm{i}Re_2(J_0 + J_E),$$

where $Re_2 = Re_1(\rho/\mu)$ is the Reynolds number of the upper fluid and

$$J_0 = \mu Q_L^2(a_2 - a_1)H_{12},$$

where

$$H_{12} = \left\{ \frac{1}{\mu}\left[H_2'(\eta_2) - \frac{2H_2(\eta_2)}{\eta_2}\right] - \frac{1}{\rho}\left[H_1'(-\eta_1) + \frac{2H_1(-\eta_1)}{\eta_1}\right] + \frac{\frac{1}{\mu}\eta_2^2 - \eta_1^2}{2(\eta_1+\eta_2)} \right.$$
$$\left. \times \left[\frac{H_2(\eta_2)}{\eta_2^2} - \frac{H_2'(\eta_2)}{\eta_2} - \frac{H_1(-\eta_1)}{\rho\eta_1^2} - \frac{H_1'(-\eta_1)}{\rho\eta_1}\right] + \frac{\eta_1}{6}\left(\eta_1 + \frac{\frac{1}{\mu}\eta_2^2 - \eta_1^2}{\eta_1+\eta_2}\right) Q_0 \right\}.$$

REFERENCES

Abdella, K. & Rasmussen, H. 1997 Electrohydrodynamic instability of two superposed fluids in normal electric fields. *J. Comput. Appl. Maths* **78**, 33–61.

Baygents, J. C. & Baldessari, F. 1998 Electrohydrodynamic instability in a thin fluid layer with an electrical conductivity gradient. *Phys. Fluids* **10** (1), 301–311.

Chen, C. H., Lin, H., Lele, S. K. & Santiago, J. G. 2005 Convective and absolute electrokinetic instability with conductivity gradients. *J. Fluid Mech.* **524**, 263–303.

Chen, K. P. 1995 Interfacial instabilities in stratified shear flows of viscous and viscoelastic fluids. *Appl. Mech. Rev.* **48**, 763–776.

Dongarra, J. J., Straughan, B. & Walker, D. W. 1996 Chebyshev tau-QZ algorithm methods for calculating spectra of hydrodynamic stability problems. *Appl. Numer. Maths* **22**, 399–434.

Glasgow, I., Batton, J. & Aubry, N. 2004 Electroosmotic mixing in microchannels. *Lab Chip* **4**, 558–562.

Hoburg, J. F. & Melcher, J. R. 1976 Internal electrohydrodynamic instability and mixing of fluids with orthogonal field and conductivity gradients. *J. Fluid Mech.* **73**, 333–351.

Hooper, A. P. 1989 The stability of two superposed viscous fluids in a channel. *Phys. Fluids* **1** (7), 1133–1142.

Hooper, A. P. & Boyd, W. G. C. 1983 Shear-flow instability at the interface between two viscous fluids. *J. Fluid Mech.* **128**, 507–528.

Joseph, D. D. & Renardy, Y. Y. 1993 *Fundamentals of Two-Fluid Dynamics, Part I: Mathematical Theory and Applications*. Springer.

Lin, H., Storey, B. D., Oddy, M. H., Chen, C. H. & Santiago, J. G. 2004 Instability of electrokinetic microchannel flows with conductivity gradients. *Phys. Fluids* **16** (6), 1922–1935.

Melcher, J. R. 1963 *Field Coupled Surface Waves*. MIT Press.

Melcher, J. R. & Schwarz, W. J. 1968 Interfacial relaxation overstability in a tangential electric-field. *Phys. Fluids* **11** (12), 2604.

Melcher, J. R. & Smith, C. V. 1969 Electrohydrodynamic charge relaxation and interfacial perpendicular-field instability. *Phys. Fluids* **12** (4), 778.

el Moctar, A. O., Aubry, N. & Batton, J. 2003 Electro-hydrodynamic micro-fluidic mixer. *Lab Chip* **3**, 273–280.

Mohamed, A. A., Elshehawey, E. F. & ElSayed, M. F. 1995 Electrohydrodynamic stability of two superposed viscous fluids. *J. Colloid Interface Sci.* **169**, 65–78.

Nagata, M. 1990 Three-dimensional finite-amplitude solutions in plane Couette flow: bifurcation from infinity. *Appl. Mech. Rev.* **217**, 519–527.

Orszag, S. A. 1971 Accurate solution of the Orr–Sommerfeld stability equation. *J. Fluid Mech.* **50**, 689.

Ozen, O., Aubry, N., Papageorgiou, D. T. & Petropoulos, P. G. 2006*a* Electrohydrodynamic linear stability of two immiscible fluids in channel flow. *Electrochim. Acta* **51**, 5316–5323.

Ozen, O., Aubry, N., Papageorgiou, D. T. & Petropoulos, P. G. 2006*b* Monodisperse drop formation in square microchannels. *Phys. Rev. Lett.* **94**, 144501.

Ozen, O., Papageorgiou, D. T. & Petropoulos, P. G. 2006*c* Nonlinear stability of a charged electrified viscous liquid film under the action of a horizontal electric field. *Phys. Fluids* **18**, 042102.

Papageorgiou, D. T. & Petropoulos, P. G. 2004 Generation of interfacial instabilities in charged electrified viscous liquid films. *J. Engng Maths* **50** (2–3), 223–240.

Papageorgiou, D. T. & Vanden-Broeck, J.-M. 2004 Large-amplitude capillary waves in electrified fluid sheets. *J. Fluid Mech.* **508**, 71–88.

Renardy, Y. 1985 Instability at the interface between two shearing fluids in a channel. *Phys. Fluids* **28** (12), 3441–3443.

Renardy, Y. 1987 The thin-layer effect and interfacial stability in a two-layer Couette flow with similar liquids. *Phys. Fluids* **30** (6), 1627–1637.

Savettaseranee, K., Papageorgiou, D. T., Petropoulos, P. G. & Tilley, B. S. 2003 The effect of electric fields on the rupture of thin viscous films by van der Waals forces. *Phys. Fluids* **15** (3), 641–652.

Saville, D. A. 1997 Electrohydrodynamics: the Taylor–Melcher leaky dielectric model. *Annu. Rev. Fluid Mech.* **29**, 27–64.

Storey, B. D., Tilley, B. S., Lin, H. & Santiago, J. G. 2005 Electrokinetic instabilities in thin microchannels. *Phys. Fluids* **17**, 018103.

Tardu, S. 2004 Interfacial electrokinetic effect on the microchannel flow linear stability. *Trans. ASME* I: *J. Fluids Engng* **126**, 10–13.

Tilley, B. S., Petropoulos, P. G. & Papageorgiou, D. T. 2001 Dynamics and rupture of planar electrified liquid sheets. *Phys. Fluids* **13** (12), 3547–3563.

Yiantsios, S. G. & Higgins, B. G. 1988 Linear stability of plane Poiseuille flow of two superposed superposed fluids. *Phys. Fluids* **31** (11), 3225–3238.

Yih, C.-S. 1967 Instability due to viscosity stratification. *J. Fluid Mech.* **27**, 337–352.